AD-A089 742 FLORIDA UNIV GAINESVILLE DEPT OF ENGINEERING SCIENCES F/G 17/9
REFLECTANCE OF SNOW AT MILLIMETER WAVELENGTHS.(U)
MAR 80 R C ANDERSON, K I MACFEELY AFOSR-77-3415
UNCLASSIFIED AFOSR-TR-80-0750 NL

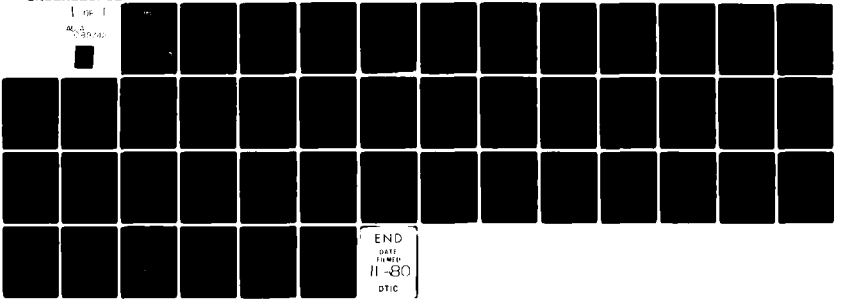

END
DATE FILMED
11-80
DTIC

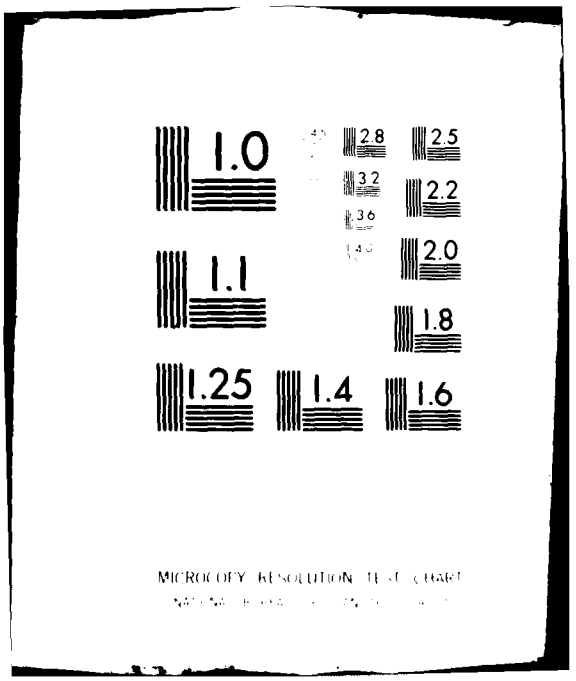
1.0
2.8
2.5
3.2
2.2
3.6
2.0
1.1
1.8
1.25
1.4
1.6
MICROCOPY RESOLUTION TEST CHART

LEVEL II

9

BS.

AD A089742

DTIC
ELECTE
SEP 26 1980
S D
C

DDC FILE COPY

80 9 25 067

UNCLASSIFIED

SECURITY CLASSIFICATION OF THIS PAGE (When Data Entered)

(19) REPORT DOCUMENTATION PAGE

READ INSTRUCTIONS BEFORE COMPLETING FORM

1. REPORT NUMBER (18) AFOSR TR-80-0750	2. GOVT ACCESSION NO. AD-A089742
3. RECIPIENT'S CATALOG NUMBER	
4. TITLE (and Subtitle) REFLECTANCE OF SNOW AT MILLIMETER WAVELENGTHS	5. TYPE OF REPORT & PERIOD COVERED Final rpt.
	6. PERFORMING ORG. REPORT NUMBER
7. AUTHOR(s) (10) R. C. Anderson, K. I. MacFeely	8. CONTRACT OR GRANT NUMBER(s) AFOSR 77-3415
9. PERFORMING ORGANIZATION NAME AND ADDRESS Department of Engineering Sciences, University of Florida, Gainesville, FL 32611	10. PROGRAM ELEMENT, PROJECT, TASK AREA & WORK UNIT NUMBERS 61102F 2301/A6 (17) A6 (16)
11. CONTROLLING OFFICE NAME AND ADDRESS AFOSR/NP, Bolling AFB, Bldg. #410, Wash DC 20332 (12) 49	12. REPORT DATE (11) 4 Mar 80
	13. NUMBER OF PAGES 44
14. MONITORING AGENCY NAME & ADDRESS (if different from Controlling Office)	15. SECURITY CLASS. (of this report) unclassified
	15a. DECLASSIFICATION/DOWNGRADING SCHEDULE

16. DISTRIBUTION STATEMENT (of this Report)

DISTRIBUTION STATEMENT A
Approved for public release;
Distribution unlimited

17. DISTRIBUTION STATEMENT (of the abstract entered in Block 20, if different from Report)

18. SUPPLEMENTARY NOTES

19. KEY WORDS (Continue on reverse side if necessary and identify by block number)

20. ABSTRACT (Continue on reverse side if necessary and identify by block number)

Radar cross sections of ground snow were calculated for linearly polarized incident radiation at 8.6, 17, 35, and 95 GHz. The snow was modeled as a plane parallel medium consisting of ice grains mixed with varying amounts of liquid water. Individual ice grains were treated as independent Rayleigh scattering centers and the water as a homogeneous absorbing medium. Calculations of the radar cross section were made using known solutions of the radiative transfer equation. These were then compared with experimental data. Curves are given which can be used to find the radar cross section given the grain size and the

DD FORM 1 JAN 73 1473

UNCLASSIFIED

SECURITY CLASSIFICATION OF THIS PAGE (When Data Entered)

water content of the snow.

AFOSR-TR- 80-0750

Final Report for AFOSR [redacted]

Reflectance of Snow at Millimeter Wavelengths

R. C. Anderson and K. I. MacFeely

Approved for public release;
distribution unlimited.

Research sponsored by the Air Force Office of Scientific Research, Air Force Systems Command, USAF, under Grant No. AFOSR-77-3415

DTIC
ELECTE
SEP 2 6 1980
D
C

March 4, 1980

AIR FORCE OFFICE OF SCIENTIFIC RESEARCH (AFSC)
NOTICE OF TRANSMITTAL TO DDC
This technical report has been reviewed and is approved for public release IAW AFR 190-12 (7b).
Distribution is unlimited.
A. D. BLOSE
Technical Information Officer

ABSTRACT

Radar cross sections of ground snow were calculated for linearly polarized incident radiation at 8.6, 17, 35, and 95 GHz. The snow was modeled as a plane parallel medium consisting of ice grains mixed with varying amounts of liquid water. Individual ice grains were treated as independent Rayleigh scattering centers and the water as a homogeneous absorbing medium. Calculations of the radar cross section were made using known solutions of the radiative transfer equation. These were then compared with experiemntal data. Curves are given which can be used to find the radar cross section given the grain size and the water content of the snow.

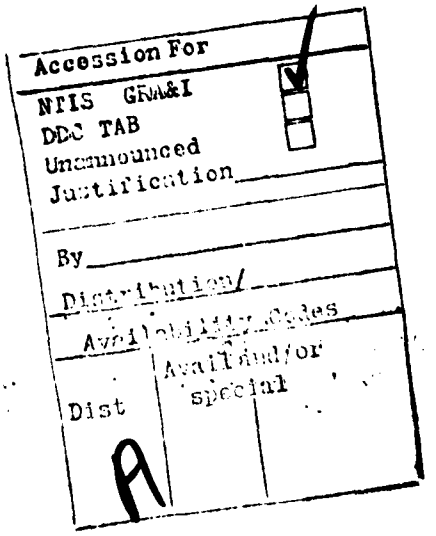

INTRODUCTION

The reflectance of ground snow at millimeter wavelengths is important for remote sensing of snow cover[1] as well as for its impact on all weather military systems. Measurements[2] show that the reflectance is strongly dependent upon the liquid water content and the illuminating beam's polarization. In addition, it has been suggested[3] that interference between reflected waves from different layers may cause considerable changes between samples.

Theoretically, snow at these wavelengths is in a radiative transfer no man's land between continua and clouds of independent scatterers - a position shared with powders[4] and paint pigments[5] because of the close packing of the grains. In this paper, the snow is taken as a cloud of Rayleigh scattering spherical ice grains interspersed with an absorbing, non-scattering medium which has characteristics similar to liquid water. Calculations have been done for direct backscatter from optically thick and optically thin snow with varying amounts of liquid water. The results are presented as plots of the variation of radar cross section with scattering angle. Several combinations of linear transmitter-receiver polarizations were considered.

SNOW MODEL

Snow is composed of a collection of irregularly shaped ice crystals packed to a wide variety of densities. The grain sizes will vary from a few microns to a millimeter or two depending upon age, previous conditions of wind, and temperature. The particles may be wetted with liquid water if the temperature is high enough. Interstitial spaces are filled with air or water. Each particle is always touching at least one neighbor. Replacing such a complex system with a cloud of independent, spherical particles immersed in an absorbing continuous medium, requires some justification.

If the particles are small compared to the wavelength, and so are Rayleigh scatterers, then the Mie scattering from a small spherical particle will look very much like that from a small irregular particle. In other words, the scattering phase function[6] is not sensitive to shape for particles very small compared to the wavelength.

Liquid water content of snow above freezing is the order of 10 percent. Its primary contribtion to this problem is caused by absorption because its absorption coefficient is approximately 500 times larger than the coefficient for ice. The water has been introduced as a continuous medium with the absorption occurring between scattering events in the multiple scattering process. Allowance has been made to account for the fact that part of the space is occupied by air.

Independent scattering is an implicit assumption in the theoretical development that will always be violated in snow. This term is used to express the idea that the flux scattered from neighboring particles will have no phase relationship. The use of such a theory was encouraged by results from the paint industry where the Kubelka-Munk (KM) theory, based on a two stream approximation, has been used for many years. It is really a two stream approximation to Chandrasekhar's[6] solution to the radiative transfer equation for plane-parallel atmospheres. The KM theory was improved by Mudgett and Richards[5] with a set of "many stream" equations. Their calculations, using four streams of radiation, showed remarkable agreement with experiment.

The related problem of long source coherence lengths has also been studied experimentally[7]. Here, a second particle is in the far field of the radiation scattered by the first but the coherence length is longer than the physical spacing. Hence, there is a phase relationship between the light scattered

from the two particles. It has been shown that this effect is averaged when scattering is caused by a suspension of randomly distributed particles.

THEORY

The snow is taken as a homogeneous plane-parallel layer with infinite lateral extent. A Cartesian coordinate system is used with the x-y plane being parallel to the snow surface and the positive z axis pointing outward. Directions are measured in spherical coordinates with θ_o and ϕ_o specifying the incident direction and θ and ϕ specifying the emergent direction.

When polarization is taken into account using Stokes parameters, the radiative transfer equation becomes a matrix equation with solutions of the form[6]

$$\mathbf{N}(\mu,\phi) = \frac{1}{4\mu}\ \mathbf{S}(\mu,\phi;\mu_o,\phi_o)\ \ \mathbf{F}(\mu_o,\phi_o) \qquad (1)$$

where

$$\mu = \cos\theta \quad , \ \mu_o = \cos\theta_o,$$

$\mathbf{N}$ is the scattered radiance [watts/cm^2 sr] Stokes vector,

$$\mathbf{N} = \begin{vmatrix} N_\ell \\ N_r \\ N_u \\ N_v \end{vmatrix} \quad , \qquad (2)$$

$\mathbf{F}$ is the irradiance [watts/cm^2] Stokes vector,

$$\mathbf{F} = \begin{vmatrix} F_\ell \\ F_r \\ F_u \\ F_v \end{vmatrix} \quad , \qquad (3)$$

and $\mathbf{S}$ is the scattering matrix. For the special case of backscattered linearly polarized light, the radar cross sections are

$$\sigma_{VV} = 4 \frac{N_\ell}{F_\ell} \quad ,$$

$$\sigma_{HH} = 4 \frac{N_r}{F_r} \qquad (4)$$

and $$\sigma_{HV} = \sigma_{VH} = 4 \frac{N_r}{F_\ell} = 4 \frac{N_\ell}{F_r} \quad .$$

Using the solutions of Abhyankar and Fymat[8] for a semi-infinite Rayleigh scattering medium, Eqs. (4) become

$$\sigma_{VV} = \frac{\omega_o}{2} \left[G_1^2(\mu_o) + G_2^2(\mu_o) + 3\,\mu_o(1-\mu_o^2) H^{(1)}(\mu_o) H^{(1)}(\mu_o) + \frac{3}{4}\,\mu_o^4\, H^{(2)}(\mu_o) H^{(2)}(\mu_o) \right] \quad , \qquad (5)$$

$$\sigma_{HH} = \frac{\omega_o}{2} \left[G_3^2(\mu_o) + G_4^2(\mu_o) + \frac{3}{4}\, H^{(2)}(\mu_o) H^{(2)}(\mu_o) \right] \quad , \quad \text{and}$$

$$\sigma_{HV} = \frac{\omega_o}{2} \left[G_1(\mu_o)\, G_3(\mu_o) + G_2(\mu_o)\, G_4(\mu_o) - \frac{3}{4}\,\mu_o^2\, H^{(2)}(\mu_o)\, H^{(2)}(\mu_o) \right]$$

where ω_o is the single scattering albedo.

The function $\mathbf{G}(\mu)$ can be found from the equation

$$\mathbf{G}(\mu) = (\mu) + \frac{1}{2}\,\omega_o\,\mu\,\mathbf{G}(\mu) \int_0^1 \mathbf{G}^T(\mu')\,\mathbf{M}(\mu')\,\frac{d\mu'}{\mu + \mu'} \qquad (6)$$

where

$$\mathbf{G}(\mu) = \begin{vmatrix} G_1(\mu) & G_2(\mu) \\ G_3(\mu) & G_4(\mu) \end{vmatrix} \quad , \qquad (7)$$

$$M(\mu) = \frac{\sqrt{3}}{2} \begin{vmatrix} \mu^2 & (1-\mu^2)\sqrt{2} \\ 1 & 0 \end{vmatrix} , \qquad (8)$$

and $G^T(\mu)$ is the transpose of $G(\mu)$. Values for the H (μ) functions can be calculated using Chandrasekhar's equation[6]

$$\frac{1}{H^{(k)}(\mu)} = \left[1 - 2\int_0^1 \psi^{(k)}(\mu')\, d\mu'\right]^{\frac{1}{2}}$$

$$+ \int_0^1 \mu' H^{(k)}(\mu') \psi^{(k)}(\mu') \frac{d\mu'}{\mu + \mu'} ; \qquad (k=1,2) \qquad (9)$$

where

$$\psi^{(1)}(\mu) = \frac{3}{8} \omega_o (1-\mu^2)(1+2\mu^2)$$

and

$$\psi^{(2)}(\mu) = \frac{3}{16} \omega_o (1+\mu^2)^2 . \qquad (10)$$

When the snow has finite optical depth, τ, and the underlying layer's albedo is zero, the radar cross sections become[9]

$$\sigma_{VV} = \frac{1}{\mu_o} S_1^{(o)}(\tau,\mu_o,\mu_o) - 3\mu_o^2(1-\mu_o^2) S_1(\tau;\mu_o,\mu_o)$$

$$+ \frac{3}{4}\mu_o^4 S_2(\tau;\mu_o,\mu_o) , \qquad (11)$$

$$\sigma_{HH} = \frac{1}{\mu_o} S_4^{(o)}(\tau;\mu_o,\mu_o) + \frac{3}{4} S_2(\tau;\mu_o,\mu_o) , \quad \text{and}$$

$$\sigma_{HV} = \frac{1}{\mu_o} S_2^{(o)}(\tau;\mu_o,\mu_o) - \frac{3}{4}\mu_o^2 S_2(\tau;\mu_o,\mu_o)$$

where the elements of the scattering matrix can be found from

$$\left(\frac{1}{\mu_o} + \frac{1}{\mu} + \frac{\partial}{\partial\tau}\right) S^{(o)}(\tau,\mu,\mu_o) = \omega_o\left[M(\mu) + \frac{1}{2}\int_0^1 S^{(o)}(\tau;\mu,\mu') M(\mu')\frac{d\mu'}{\mu'}\right]\left[M^T(\mu_o) + \frac{1}{2}\int_0^1 M^T(\mu'') S^{(o)}(\tau;\mu'',\mu_o)\frac{d\mu'}{\mu''}\right] \quad (12)$$

and

$$\left(\frac{1}{\mu_o} + \frac{1}{\mu} + \frac{\partial}{\partial\tau}\right) S_k(\tau;\mu,\mu_o) = \omega_o\left[1 + \int_0^1 \Psi^k(\mu') S_k(\tau;\mu,\mu^1)\frac{d\mu'}{\mu'}\right] \quad (13)$$

$$X\left[1 + \int_0^1 \Psi^k(\mu'') S_k(\tau;\mu_o,\mu'')\frac{d\mu''}{\mu''}\right]; \quad (k=1,2).$$

Optical Depth and Single Scattering Albedo

The effects of the snow's physical properties will be determined by the single scattering albedo, ω_o, and the optical depth, τ. The single scattering albedo is defined as

$$\omega_o = \frac{\beta_{sc}}{\beta_{ex}} = \frac{\beta_{sc}}{\beta_{sc} + \beta_{ab}} \quad (14)$$

where β_{sc} is the scattering coefficient, β_{ab} is the absorption coefficient, and β_{ex} is the extinction coefficient. Since water is being treated as contributing only to the absorption, the scattering coefficient is the scattering

coefficient for ice particles. The absorption coefficient for the mixture becomes

$$\beta_{ab} = \beta_{ab,i} + \beta_{ab,w} \tag{15}$$

where $\beta_{ab,i}$ is absorption coefficient for ice and $\beta_{ab,w}$ is the absorption coefficient for liquid water. After substituting these values into Eq. 14 and dividing the numerator and denominator through by $\beta_{sc,i}$, the single scattering albedo for the mixture becomes

$$\omega_o = \frac{1}{\frac{1}{\omega_{o,i}} + \frac{\beta_{ab,w}}{\beta_{sc,i}}} \tag{16}$$

where $\omega_{o,i}$ is the single scattering albedo for the ice spheres.

Looking at the last term in the denominator, the scattering coefficient for ice particles in the snow can be written as[10]

$$\beta_{sc,i} = \pi a^2 Q_{sc,i} n_{i,s} \tag{17}$$

where a is a mode radius presumed to represent the ice particles, $Q_{sc,i}$ is the particle scattering efficiency factor and $n_{i,s}$ is the average number of ice particles per unit volume of snow. Starting with the absorption coefficient of liquid water, K_w, the absorption coefficient for the water in the snow is written as a proportion of K_w, or

$$\beta_{ab,w} = \frac{K_w n_{w,s}}{n_w} \tag{18}$$

where $n_{w,s}$ is the number of liquid water molcules per unit volume of snow and n_w is the number density of water. The ratio of the two number densities can be written

$$\frac{n_{w,s}}{n_w} = \frac{C \rho_s}{\rho_w} \tag{19}$$

where ρ_s is the density of the snow, ρ_w is the density of liquid water and C is the ratio of the density of water in the snow to the density of the snow. The density of the ice particles, is taken as

$$\rho_{i,s} = \frac{4}{3} \pi a^3 \rho_i n_{i,s} = \rho_s (1-C) \tag{20}$$

where ρ_i is the density of ice. Using Eqs. 19 and 20, the absorption coefficient for water in the snow becomes

$$\beta_{ab,w} = \frac{4}{3} \frac{\pi a^3 K_w C \rho_i n_{i,s}}{(1-C) \rho_w} \tag{21}$$

After substitution of Eqs. 17 and 21 into Eq. 16, the single scattering albedo of the snow can be written as

$$\omega_o = \frac{1}{\frac{1}{\omega_{o,i}} + \frac{4 aK_w C \rho_i}{3 (1-C) \rho_w Q_{sc,i}}} \tag{22}$$

The optical depth is defined as[6]

$$\tau = \int_0^z \beta_{ex} (z) \, dz \tag{23}$$

where z is the perpendicular depth of the snow. If the extinction coefficient is constant with depth, Eq. 23 becomes

$$\tau = z \beta_{ex} = (\beta_{ex,i} + \beta_{ab,w}) z \tag{24}$$

Writing the extinction coefficient for ice in the same form as the scattering coefficient in Eq. 17 and using Eq. 21 for the water absorption coefficient, the optical depth becomes

$$\tau = z n_{i,s} \pi a^2 \left(Q_{ex,i} + \frac{4aK_w C \rho_i}{3 (1-C)\rho_w} \right) \tag{25}$$

for a monodispersion of ice particles with mode radius a.

CALCULATIONS

Calculation of the radar cross section starts with the single scattering albedo given by Eq. 22. Values for the absorption coefficients were found from the equation

$$K_w = \frac{4\pi m}{\lambda} \tag{26}$$

where λ is the wavelength of the incident radiation and m is the imaginary part of the complex refractive index for water. The values for m, given by Ray,[11] were used. The single scattering albedo, scattering efficiency factor, and extinction efficiency factor for ice spheres were calculated with the Dave[12] routine for Mie scattering. Absorption coefficients, scattering efficiency factors, and the single scattering albedos for ice were combined to find the single scattering albedos of snow at 8.6, 17, 35 and 95 GHz for particle radii varying from 0.1 to 1.0 mm. The results are plotted, in Figs. 1 to 4, as a function of the percent liquid water content by weight.

Calculations of the optical depth required a knowledge of the ice particle number density. This was found from the relationship

$$n_i = \frac{\rho_s}{\rho_i V_i}$$

where V_i is the volume of a single ice sphere. The density of the snow, taken to be $0.45 g/cm^3$, was assumed to be constant with changes in the liquid water content. Optical depths for the four frequencies are listed in Tables I to IV for radii of 0.1, 0.5 and 1.0 mm and free water contents from 0 to 30 percent by weight.

With the single scattering albedo and the optical depth known, calculations of the radar cross section, as a function of scattering angle, can be made. The results are shown for semi-infinite layers in Figs. 5, 6, and 7 for the three different linear polarizations. The single scattering albedos were varied from 0.01 to 0.999 for VV and HH polarizations. They varied from 0.1 to 0.999 for the HV polarizations.

Similar families of curves are given in Figs. 8 to 19 for finite optical depths of 0.1, 0.5, 1.0 and 5.0 with single scatterings albedos of 0.1, 0.5, and 1.0. The underlying albedo is taken equal to zero. For optical thicknesses greater than 5.0 and modest incident angles, values of the radar cross section for the semi-infinite case approximate those with finite thicknesses. At large scattering angles, the differences between finite and semi-infinite cases increase.

Diurnal variations in the experimentally measured radar cross sections and free water content,[2] along with theoretically calculated cross sections, appear in Figs. 20 and 21. The reported free water content was measured in the top 10 cm of a layer about 20 to 30 cm deep at the time of the measurements. The snow was old and so had been through many melt-freeze cycles. Measurements of these experimental cross sections were made at incident angles of 75 and 78 degrees using linearly polarized, 35 GHz radiation.

Theoretical cross sections were calculated for comparison using the reported free water content and an assumed particle radius. The radius was determined by first selecting a single scattering albedo from Fig. 6 which gave a theoretical cross section equal to the experimental cross section in Fig. 20 at 0700. This value of the albedo was used in Fig. 3, with the amount of free water of 0700, to select a value for the radius. Following this procedure, a radius of 0.5 mm was found to fit the data from Fig. 20 and a

radius of 0.6 mm to fit the data in Fig. 21. With these radii and the measured free water contents, Fig. 3 was used to calculate single scattering albedos throughout the day. These albedos were in turn used in Fig. 6 to calculate the diurnal variation of the radar cross section.

The cross sections were calculated using the curves for the semi-infinite model because the snow was quite deep when measured in units of optical depth. Cross sections for HH and VV polarizations in this case are virtually equal when incident angles and albedos are the same. Hence, only one set of points is shown for the theoretical cross sections in Figs. 20 and 21.

Measurements were also available[13] for cross sections with the transmitter and receiver crossed polarized. The results showed the same type of variation with free water as the HH polarized cross sections, but at a value about 10 db lower. Calculated cross sections had a similar variation albeit 10 db too low. Other measurements have also been made[13] with an incident angle of 25° using frequencies of 8.6, 17.0, and 35.6 GHz. These are shown in Fig. 22 with theoretical curves superimposed. The curves were normalized to a point on the 17.0 GHz curve at 1600. In this case the theoretical calculations were made using the reported diurnal variation of the free water in the top 5 cm of the snow. The depth of the snow was 20 cm and so was treated as being semi-infinite. The same radius of 0.5 mm. was assumed since measurements were not available on particle sizes. The radii could not be determined as they were before because the returned power was given on a relative scale. With values for the diurnal variation in free water content and the assumed radius, Figs. 1, 2, and 3 were used to calculate the single scattering albedos, and then Fig. 6 was used to calculate the radar cross sections. All three theoretical curves are relative to the same normalization point mentioned above.

DISCUSSION OF RESULTS

Some of the variations in the radar cross sections can be expected from trends in the single scattering albedo and optical depths. At the four frequencies used, small amounts of water in the snow produce large changes in ω_o and τ.

The variations of the cross sections produced by these changes can be very complicated. When the snow is deep enough to be treated as a semi-infinite layer, ω_o will be the only parameter to produce variations in the cross section. An increase in the water content from 0 to 5 percent decreases ω_o by one or two orders of magnitude while the cross section is reduced the order of 20 db.

Tables I to IV, listing the optical depth per centimeter of snow, indicates that there can be tremendous differences in the depths required for the layer to be optically thick when the snow is dry. Being optically thick is the requirement necessary for the reflection from the underlying surface to be ignored. When the snow is wet, very thin layers will meet this condition.

Referring to Fig. 20, the mode radius required to match the measured cross section at 0700 was a very reasonable value based upon an observers description of the snow. This would seem to indicate that the theory used in this paper is capable of predicting the order of magnitude of the returned power. The run of the theoretical curve with the measured points suggests that the liquid water has also been accounted for in a reasonable way. The disparity between the calculations for the tim 0800 to 0900 is thought to be caused by the inability to measure the water content. This idea is strengthened by the fact that the measured water content stayed at 3 percent from 0630 to 0830 while the measured returns began dropping at about 0745. More than likely, this is the result of measuring an average water content in a 10 cm

layer while the returns were being affected by the top 1 or 2 cm. Figure 21 shows an even better match with similar data.

Based upon the data in Fig. 22, the methods used here do not predict well, the cross sections at one wavelength from the cross sections measured at another. However, the data are very sparse so that it is hoped that the situation will improve as more measurements become available.

The predicted angular dependence of the cross sections does not seem to agree with the data. At the single scattering albedos expected, theory predicts almost no angular variation. This does not appear to be the case in practice. Although the data are very sketchy, the trend is a decrease in the return with increasing nadir angle. It is thought that the difference is probably caused by a breakdown in the independent scattering assumption. More data are required for a proper evaluation.

CONCLUSIONS

The model developed here predicts well how the radar cross sections will change as a function of liquid water content. The absolute scale is good if the correct mode radius is selected to represent the snow. Whether or not this radius is related to the actual snow grain size will require more detailed information on the grain sizes at future measurement sites.

Shortcomings show up in the results for crossed polarized returns and the angular dependence. Crossed polarized returns are too low by 10 db when compared to available data. These calculations also indicate that the snow reflectance should not vary much with nadir angle, particularly for the lower single scattering albedos. This too does not correspond to available observations.

In spite of the difficulties, the calculated curves offer a means of finding an estimate for the radar cross sections, at 8.6, 17, 35, and 95 GHz,

for varying snow conditions. With more field work, it will probably be possible to predict, with useful accuracy, returns for HH and VV polarizations given a description of the snow.

1. K. F. Kunzi, A. D. Fisher, and D. H. Staelin, JGR, 8, 4965 (1978).

2 N. C. Currie, J. R. Teal, Jr., and F. B. Dyer, AFATL-TR-77-4, Air Force Armament Laboratory, Eglin Air Force Base (1976).

3. W. I. Linlor and G. R. Jiracek, J. of Glaciology, 14, 501 (1975).

4. A. G. Ernslie and J. R. Aronson, Appl. Opt., 12, 2585 (1973).

5. P. S. Mudgett and L. W. Richards, Appl. Opt., 10, 1503 (1971).

6. S. Chandrasekhar, "Radiative Transfer", Dover Publications, Inc. New York, (1950).

7. L. Carrier and L. Nugent, Appl. Opt. 4, 1451 (1965).

8. D. D. Abhyankar and A. L. Fyrmat, Ap. J. Suppl., 23, 35 (1971).

9. C. N. Adams and G. M. Kattawar, J. Quant. Spectrosc. Rad. Transf., 10, 341 (1970).

10. H. C. Van deHulst, Light Scattering by Small Particles, Wiley, New York, (1957).

11. P. S. Ray, Appl. Opt. 11, 1836, (1972).

12. J. V. Dave, IBM J. Res. Dev. 13, 302 (1969).

13. H. Stiles and F. Ulaby, Univ. of Kansas Center for Research Inc., Remote Sensing Lab. Report 340-1 (1977).

Table I. Optical Depth Per Centimeter of Snow at 8.6 GHz

Percent Free Water	Particle Radii 0.1 mm	0.5 mm	1.0 mm
0	0.011	0.011	0.001
5	0.169	0.169	0.017
10	0.344	0.345	0.035
15	0.540	0.541	0.054
20	0.761	0.762	0.076
25	1.011	1.013	0.101
30	1.297	1.299	0.130

Table II. Optical Depths Per Centimeter of Snow at 17.0 GHz

Percent Free Water	Particle Radii 0.1 mm	0.5 mm	1.0 mm
0	0.002	0.007	0.003
5	0.463	0.467	0.049
10	0.974	0.978	0.100
15	1.544	1.549	0.157
20	2.186	2.192	0.222
25	2.913	2.920	0.294
30	3.745	3.752	0.378

Table III. Optical Depths Per Centimeter of Snow at 35.0 GHz

Percent Free Water	Particle Radii 0.1 mm	0.5 mm	1.0 mm
0	0.004	0.069	0.056
5	1.064	1.130	0.162
10	2.241	2.308	0.279
15	3.557	3.625	0.411
20	5.038	5.107	0.559
25	6.715	6.787	0.727
30	8.633	8.706	0.919

Table IV. Optical Depth Per Centimeter of Snow at 95.0 GHz

Percent Free Water	Particle Radii 0.1 mm	0.5 mm	1.0 mm
0	0.032	3.642	1.209
5	2.189	5.801	1.425
10	4.586	8.200	1.665
15	7.264	10.882	1.933
20	10.278	13.898	2.234
25	13.693	17.317	2.576
30	17.596	21.224	2.967

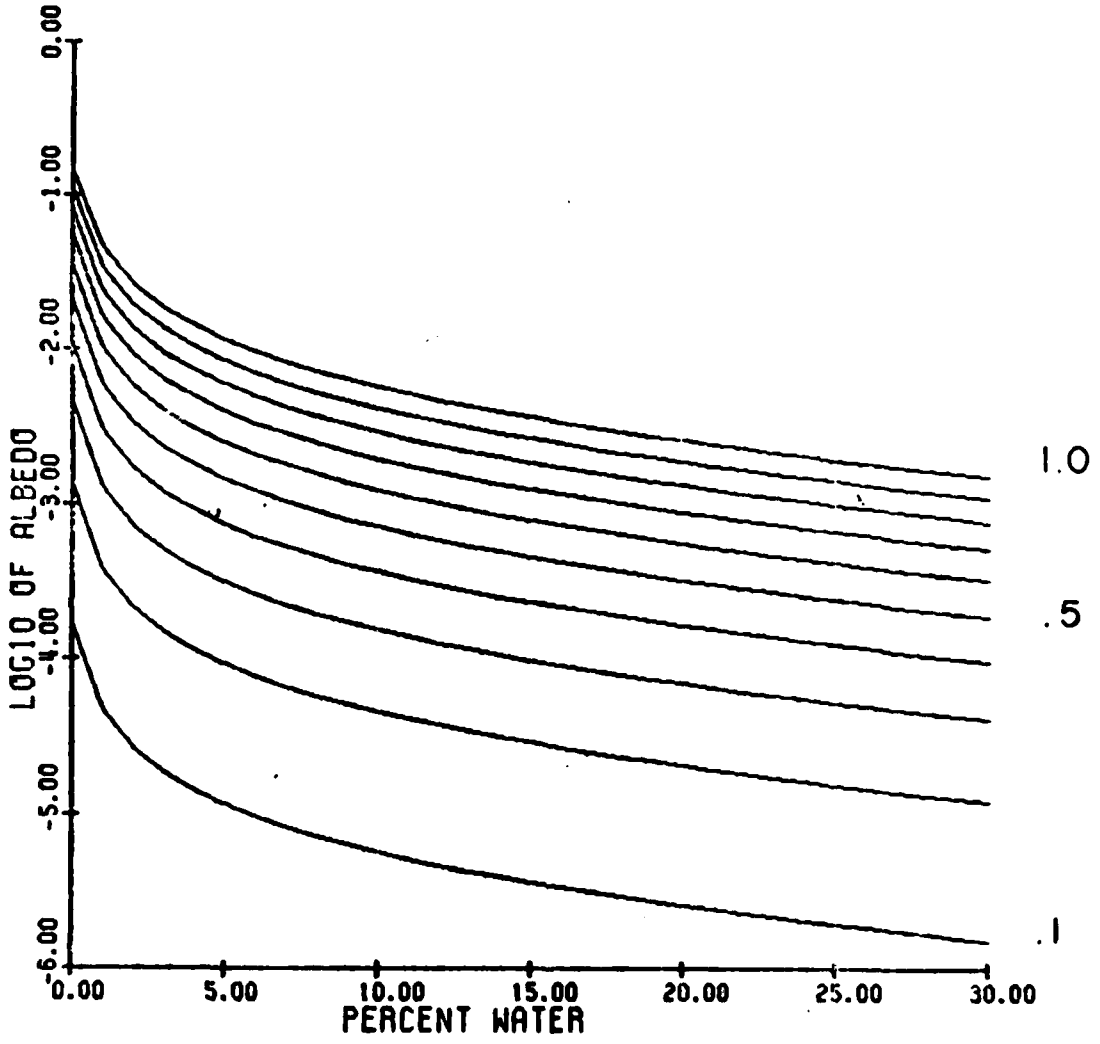

Fig. 1. Single scattering albedo versus percent free water for particles with radii between 0.1 mm and 1.0 mm at a frequency of 8.6 GHz.

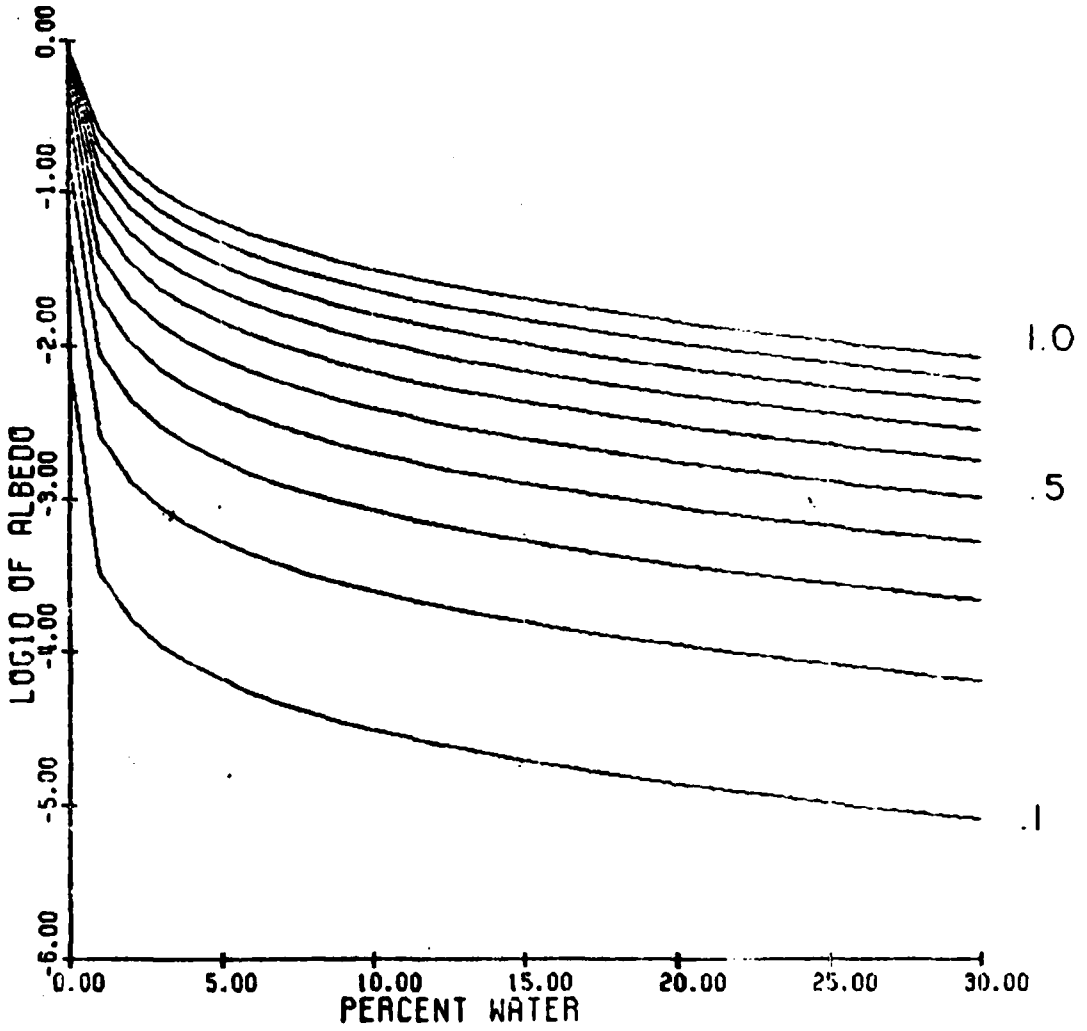

Fig. 2. Single scattering albedo versus percent free water for particles with radii between 0.1 mm and 1.0 mm at a frequency of 17 GHz.

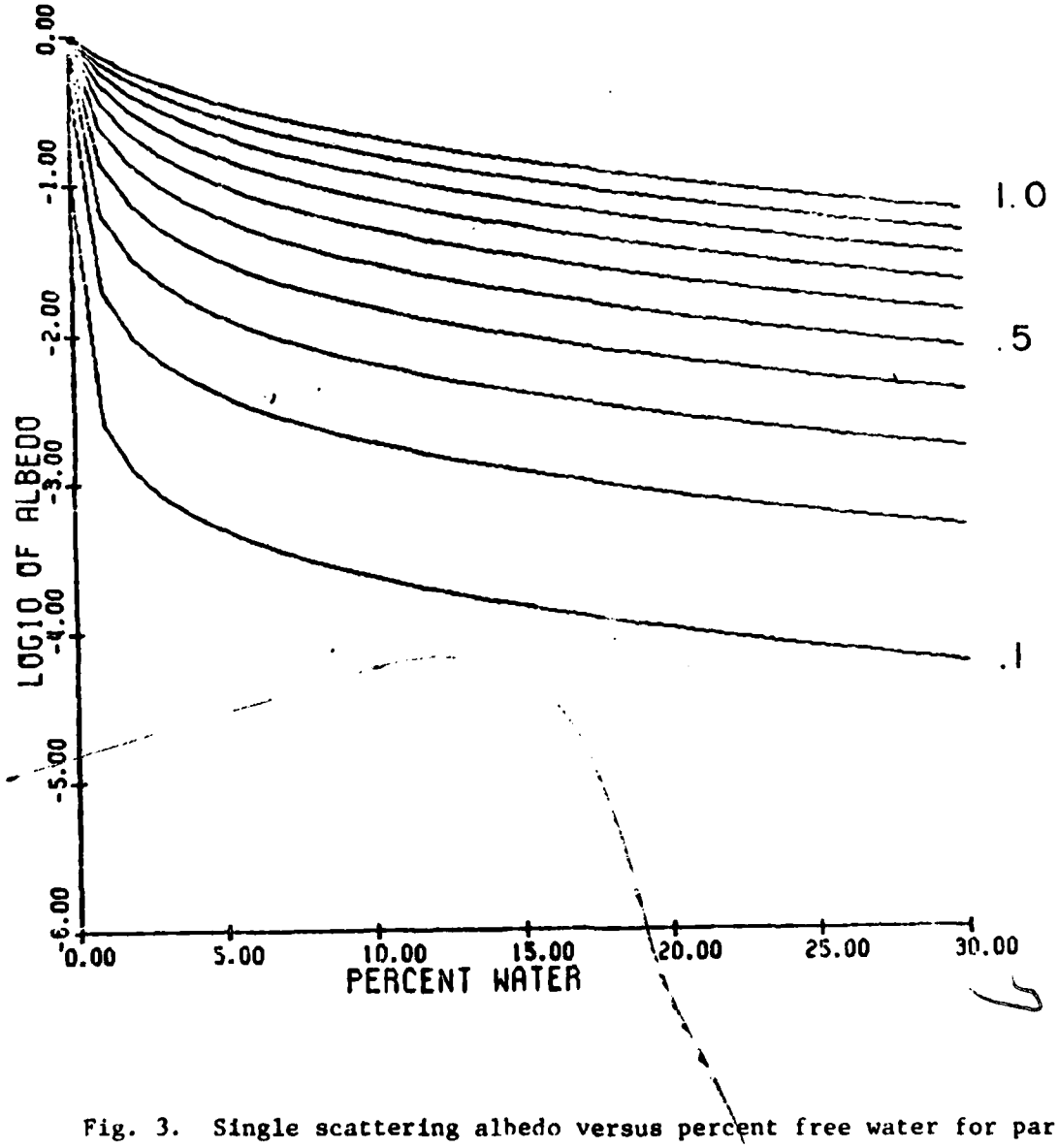

Fig. 3. Single scattering albedo versus percent free water for particles with radii between 0.1 mm and 1.0 mm at a frequency of 35.0 GHz.

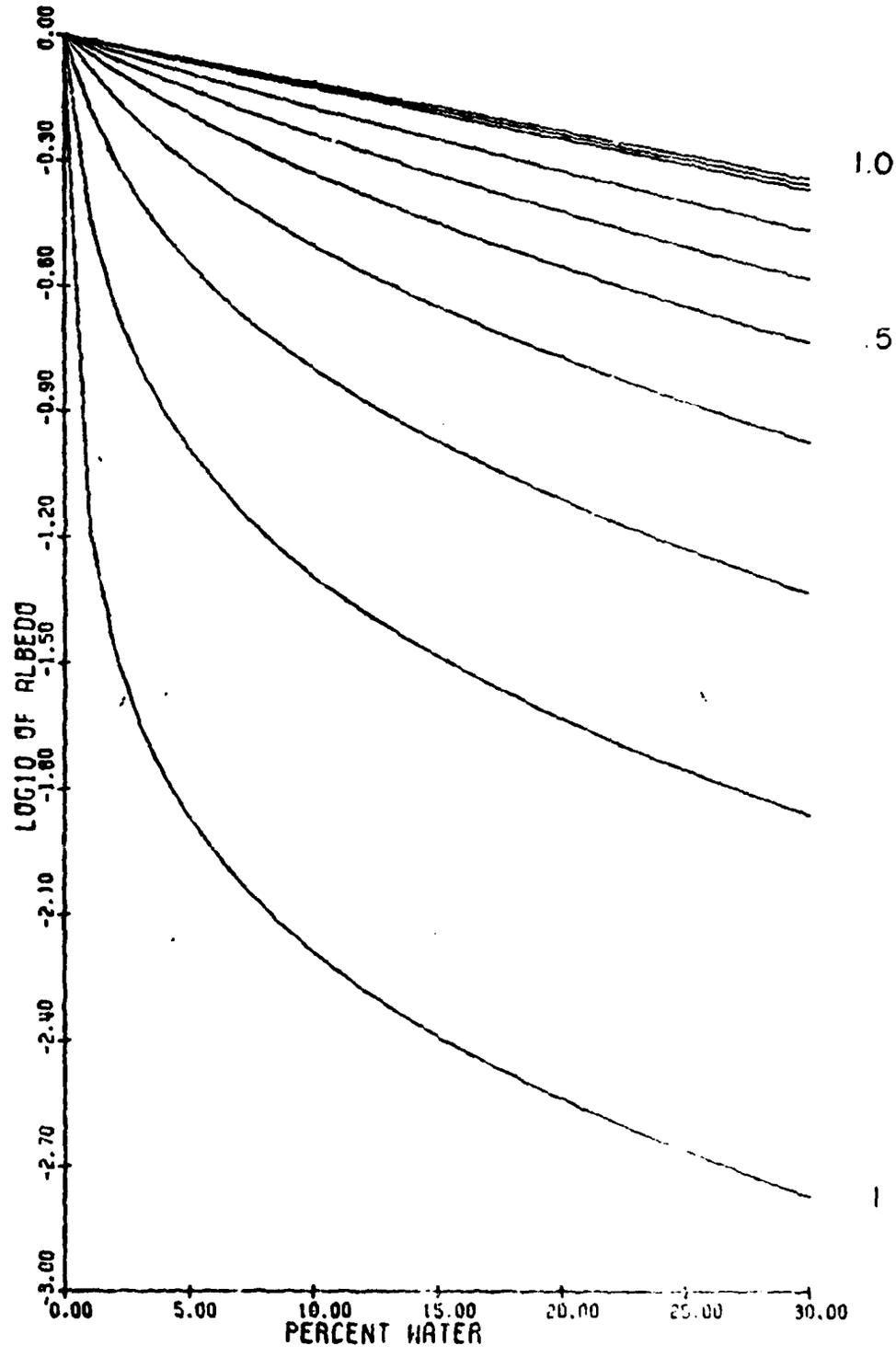

Fig. 4. Single scattering albedo versus percent free water for particles with radii between 0.1 mm and 1.0 mm at a frequency of 95.0 GHz.

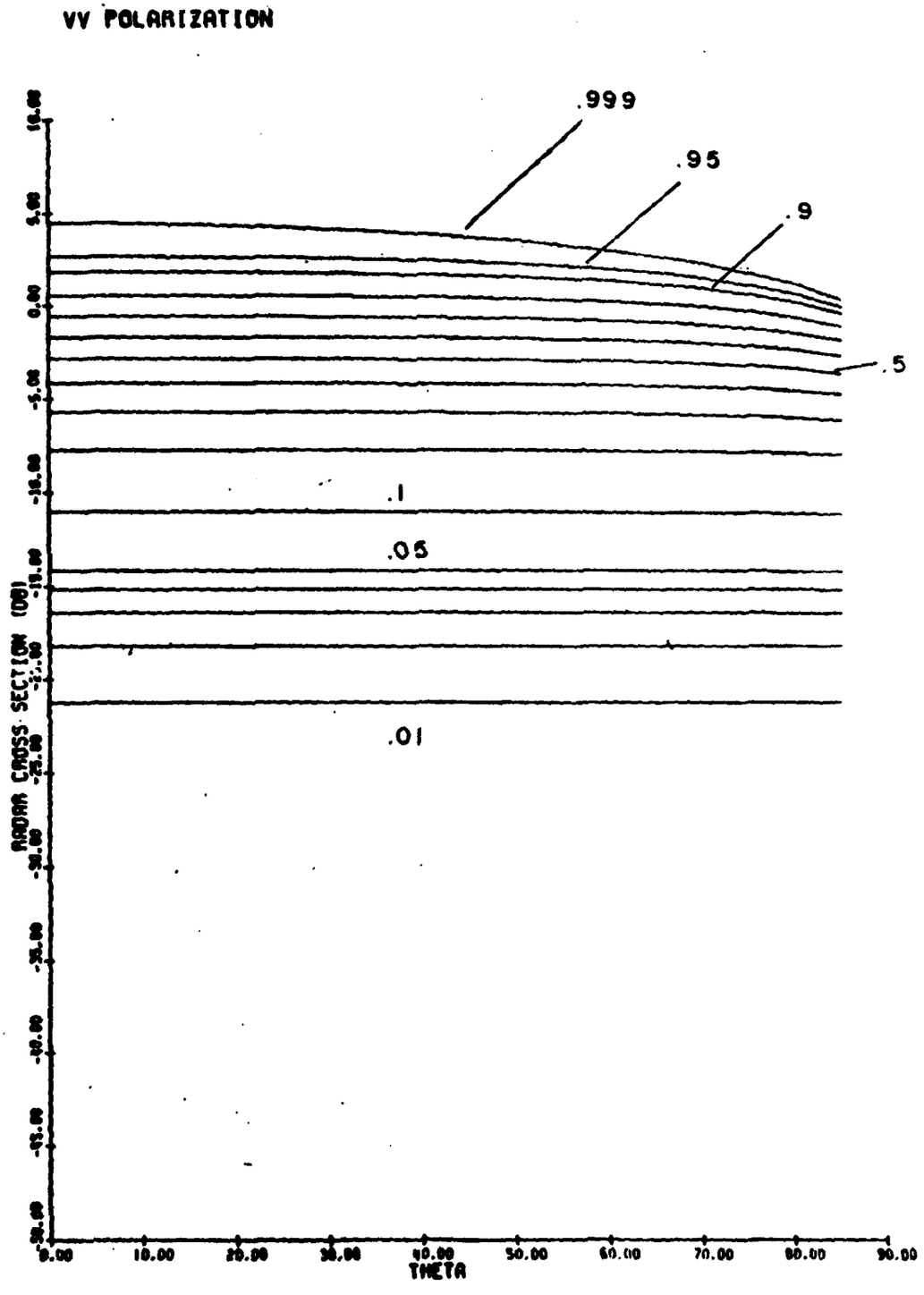

Fig. 5. Radar cross section with VV polarization versus incident angle with single scattering albedoes varying from .01 to .999.

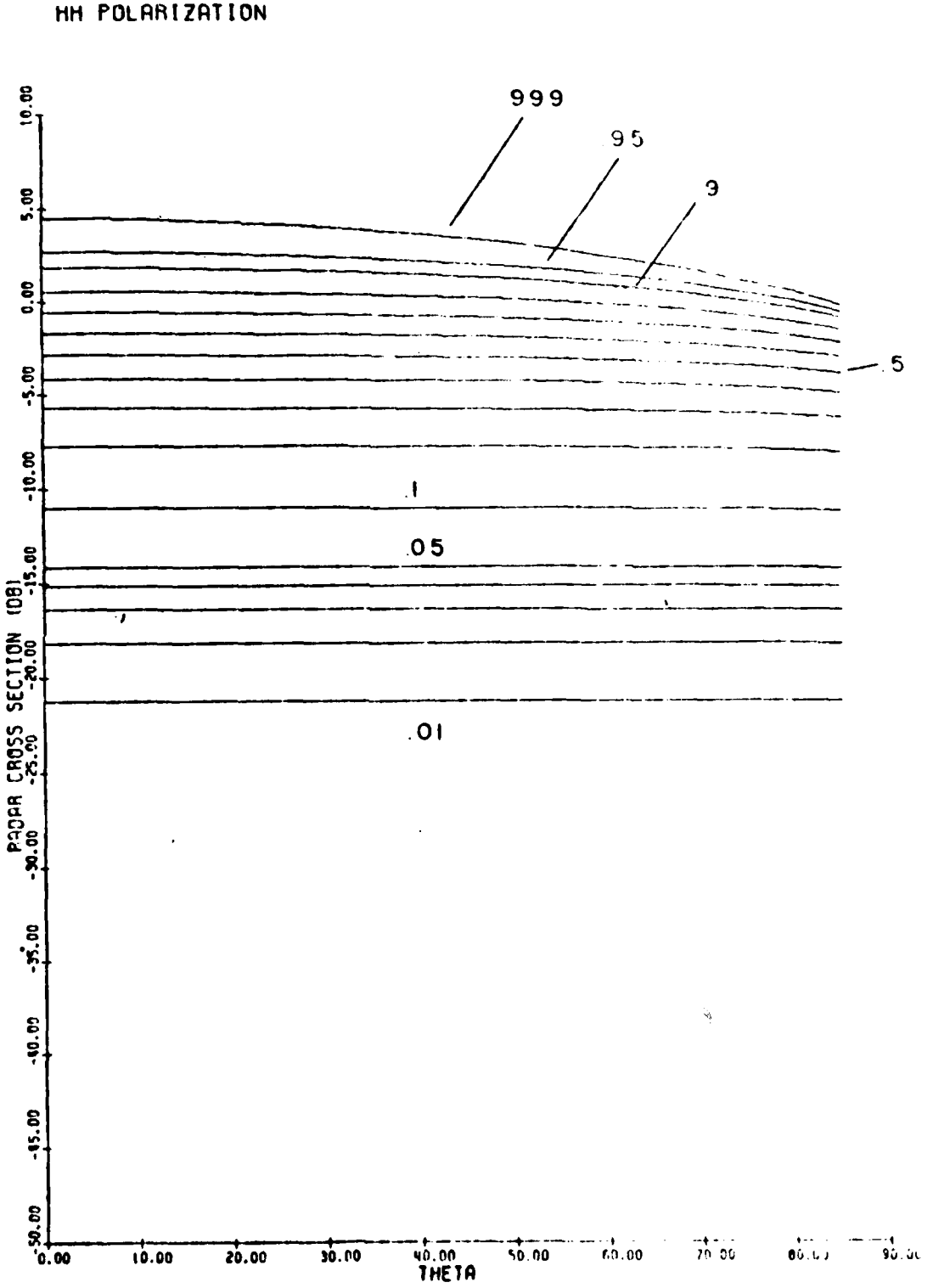

Fig. 6. Radar cross section with HH polarization versus incident angle with single scattering albedoes varying from .01 to .999.

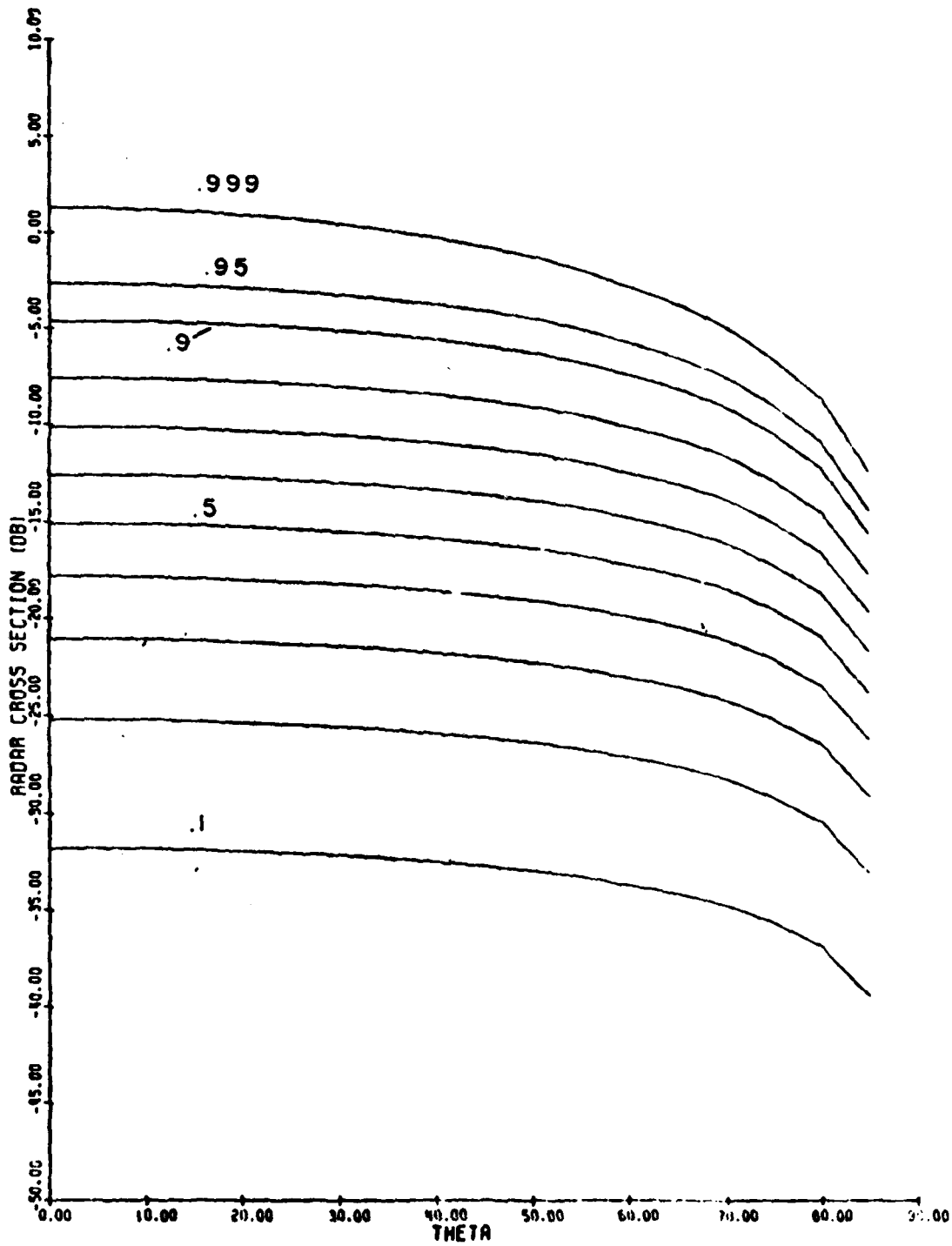

Fig. 7. Radar cross section with HV or VH polarization versus incident angle with single scattering albedoes varying from .1 to .999.

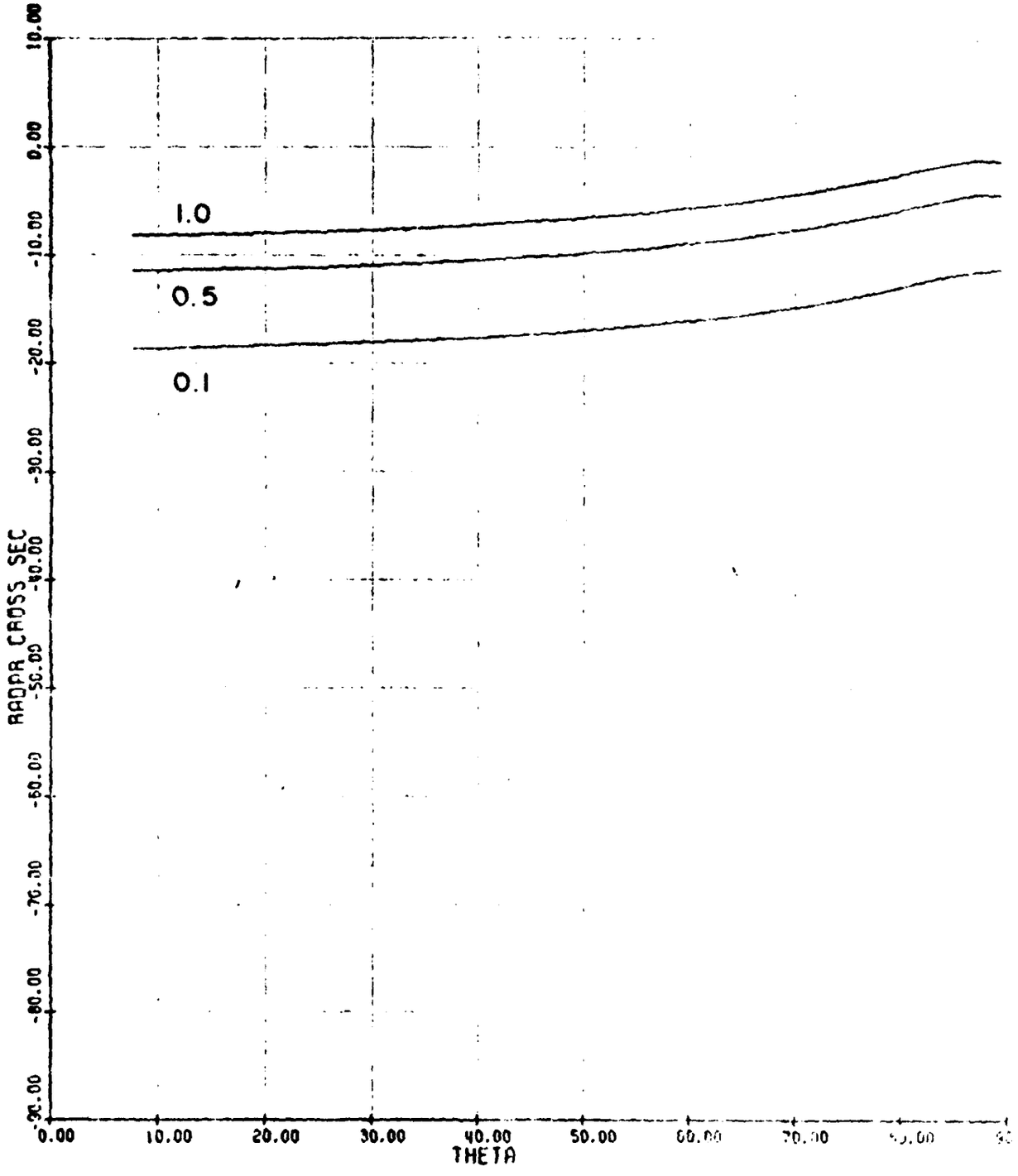

Fig. 8. Radar cross section with HH polarization versus incident angle with single scattering albedoes of .1, .5, and 1.0 for an optical depth of .1.

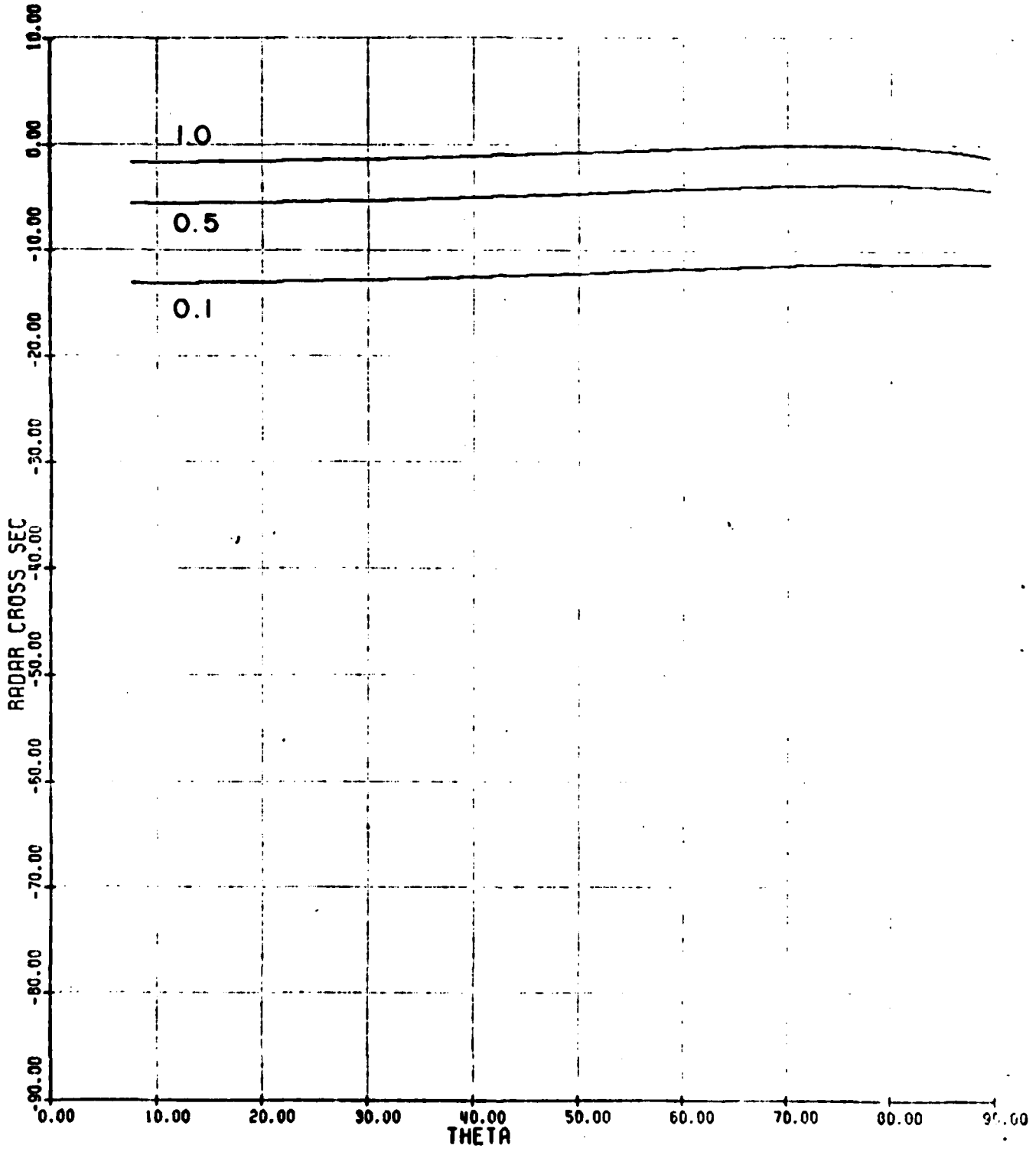

Fig. 9. Radar cross section with HH polarization versus incident angle with single scattering albedoes of .1, .5, and 1.0 for an optical depth of .5.

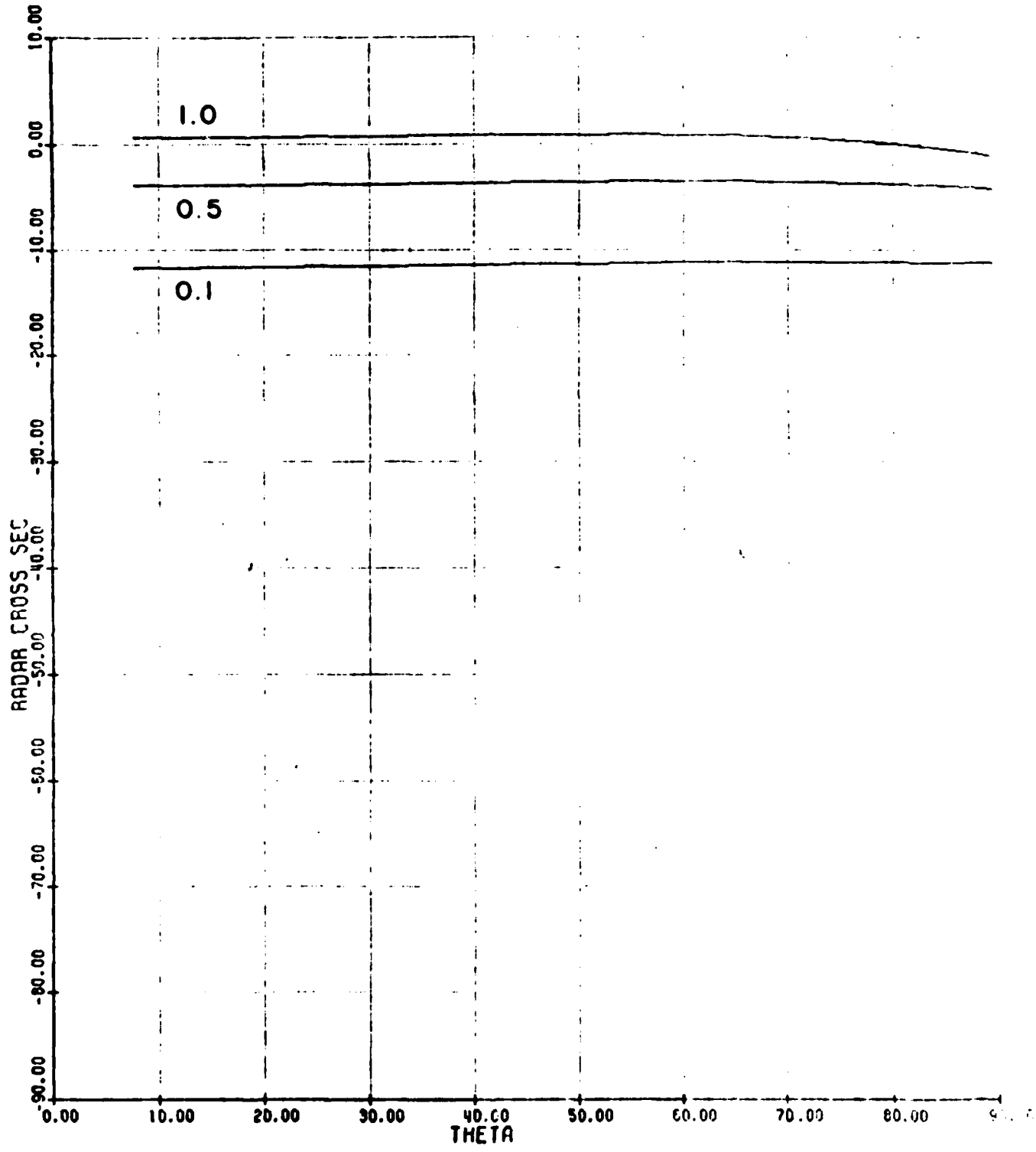

Fig. 10. Radar cross section with HH polarization versus incident angle with single scattering albedoes of .1, .5, and 1.0 for an optical depth of 1.0.

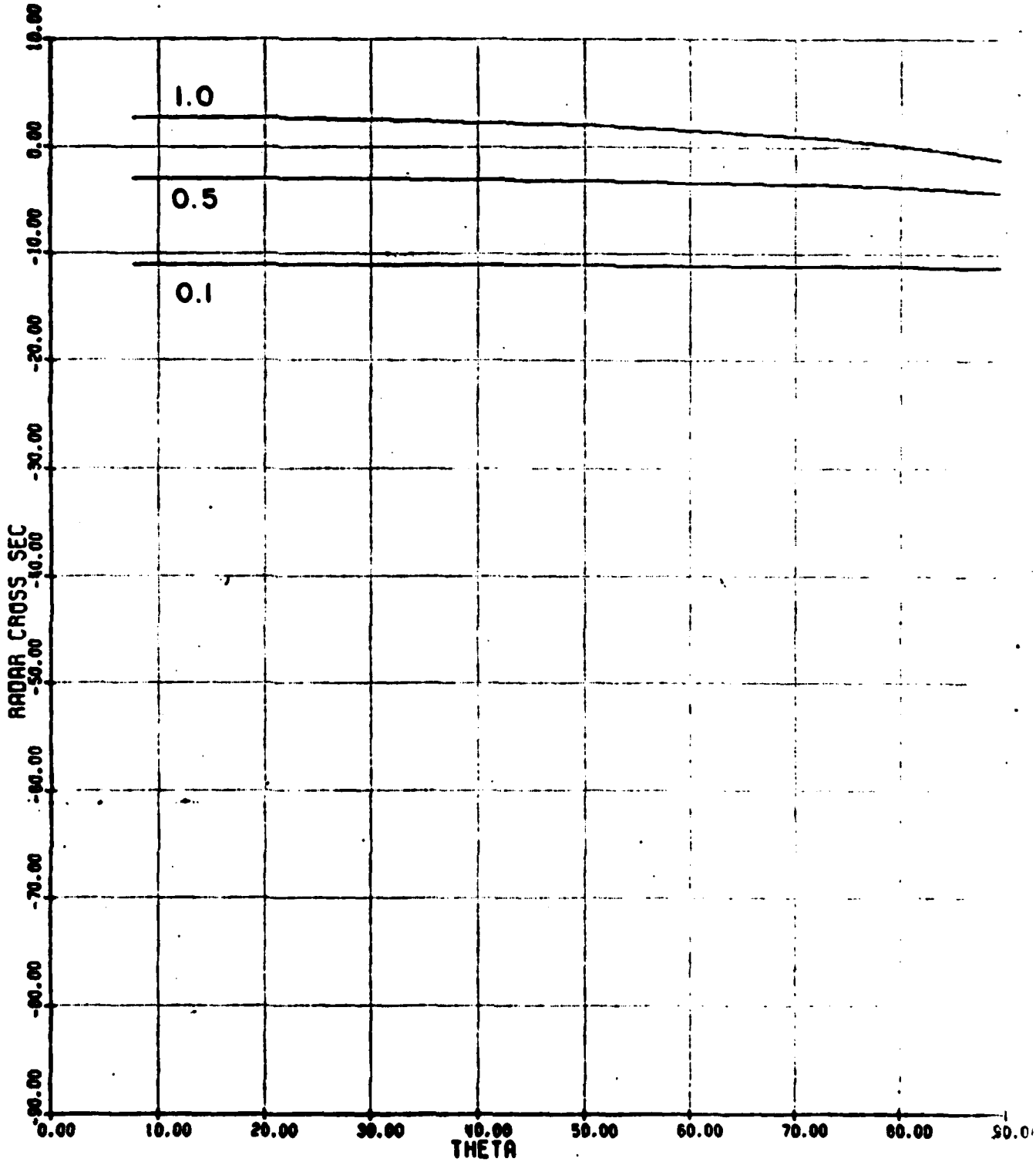

Fig. 11. Radar cross section with HH polarization versus incident agnle with single scattering albedoes of .1, .5, and 1.0 for an optical depth of 5.0.

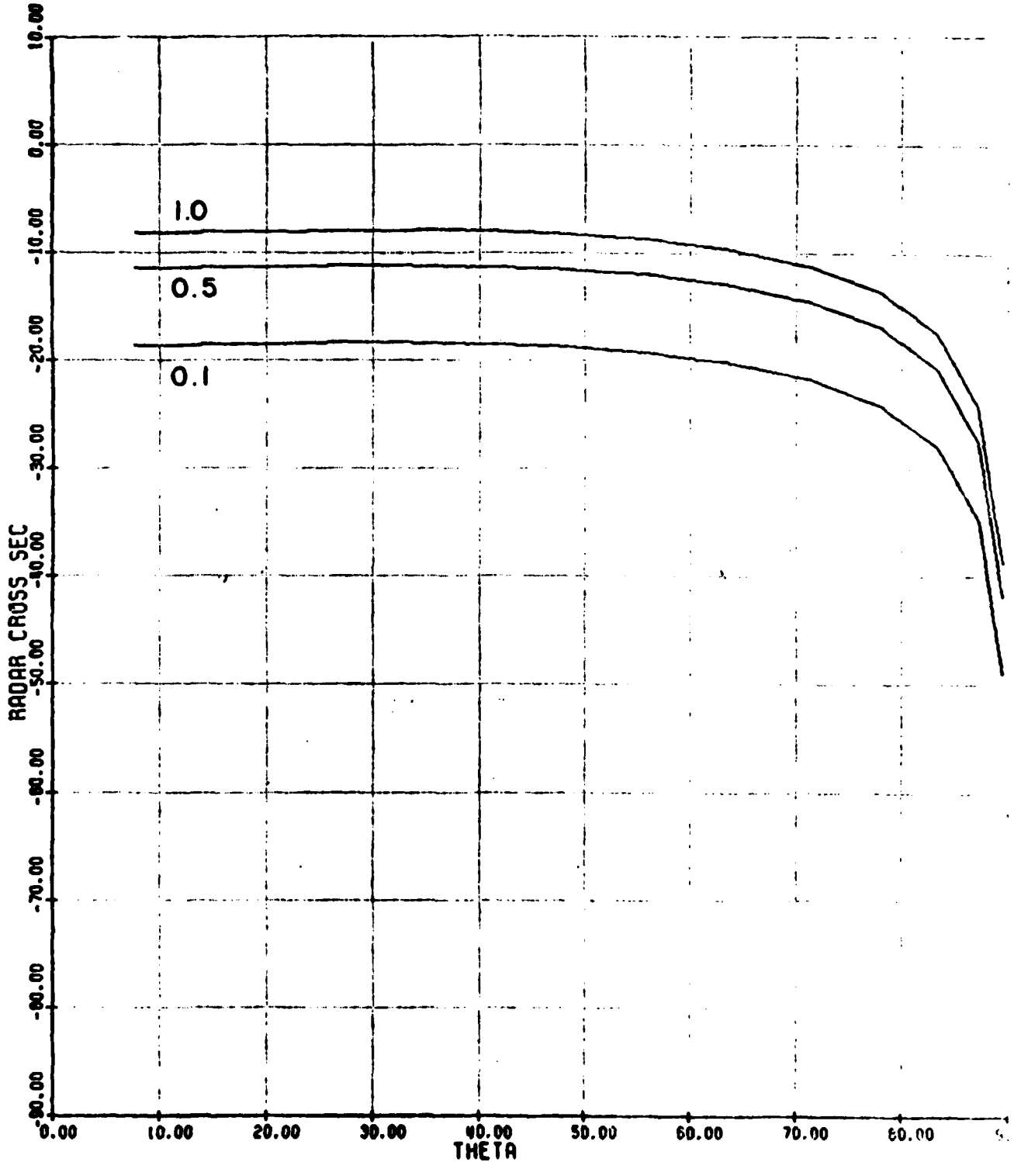

Fig. 12. Radar cross section with VV polarization versus incident angle with single scattering albedoes of .1, .5, and 1.0 for an optical depth of .1.

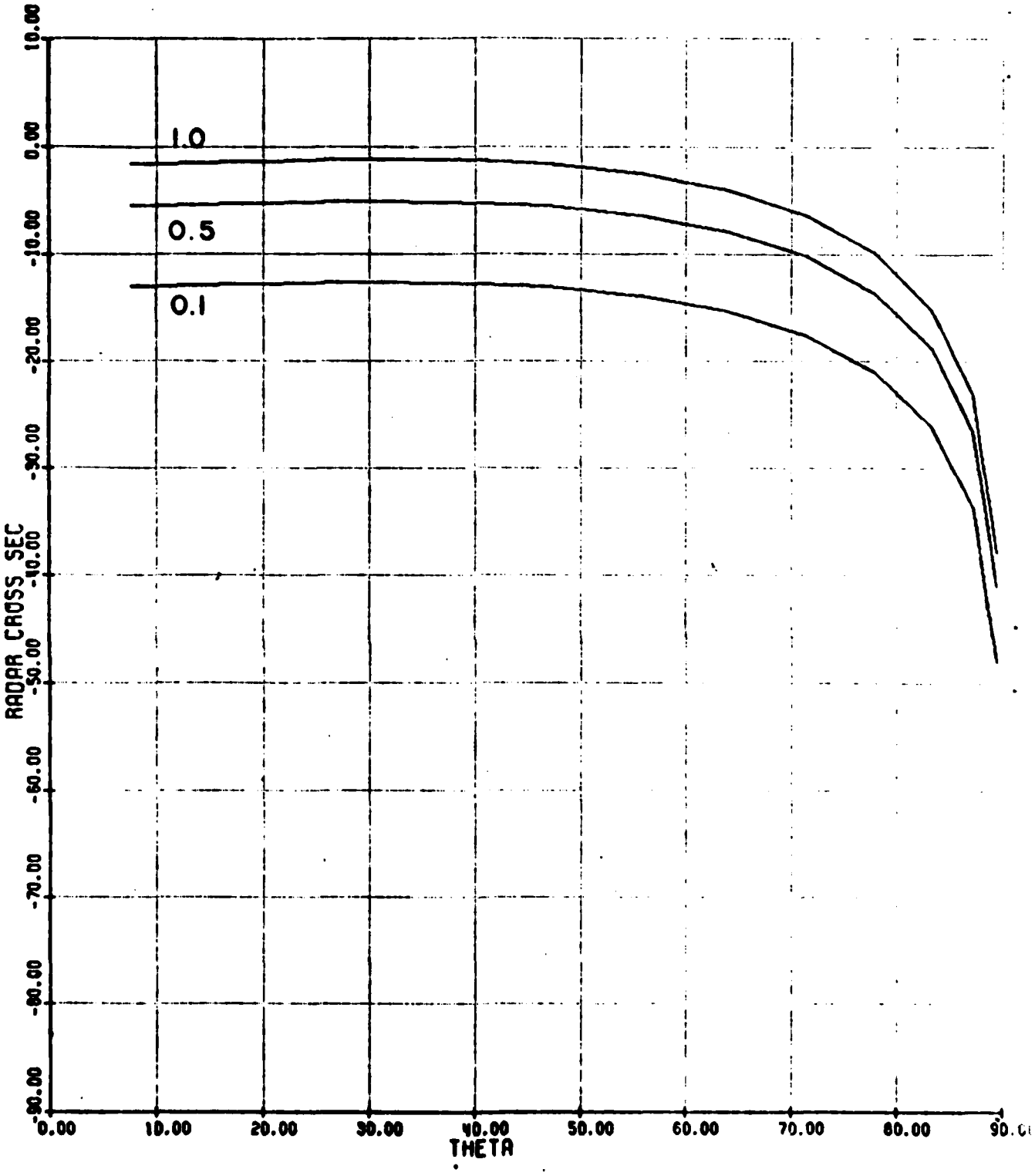

Fig. 13. Radar cross section with VV polarization versus incident angle with single scattering albedoes of .1, .5, and 1.0 for an optical depth of .5.

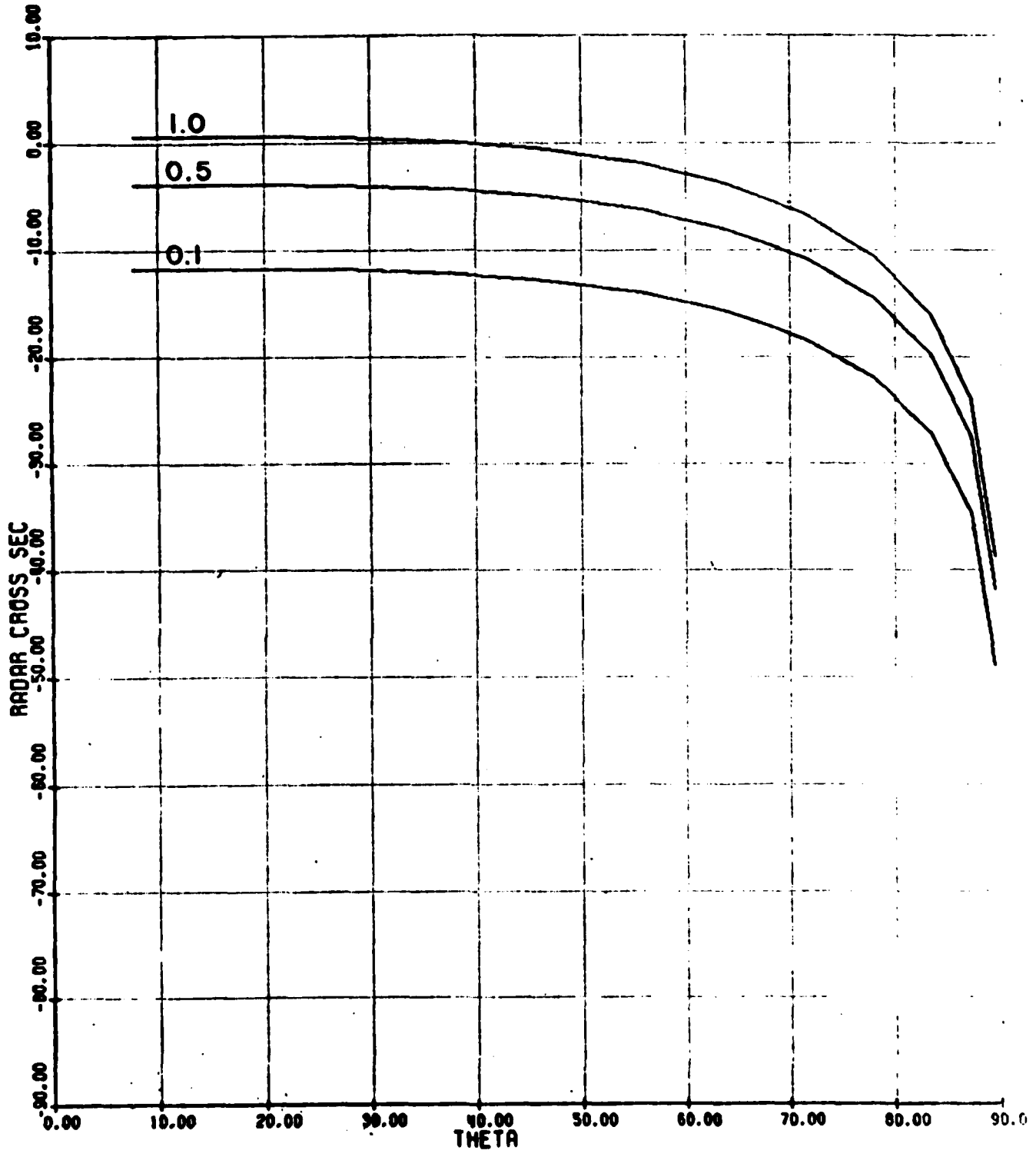

Fig. 14. Radar cross section with VV polarization versus incident angle with single scattering albedoes of .1, .5, and 1.0 for an optical depth of 1.0.

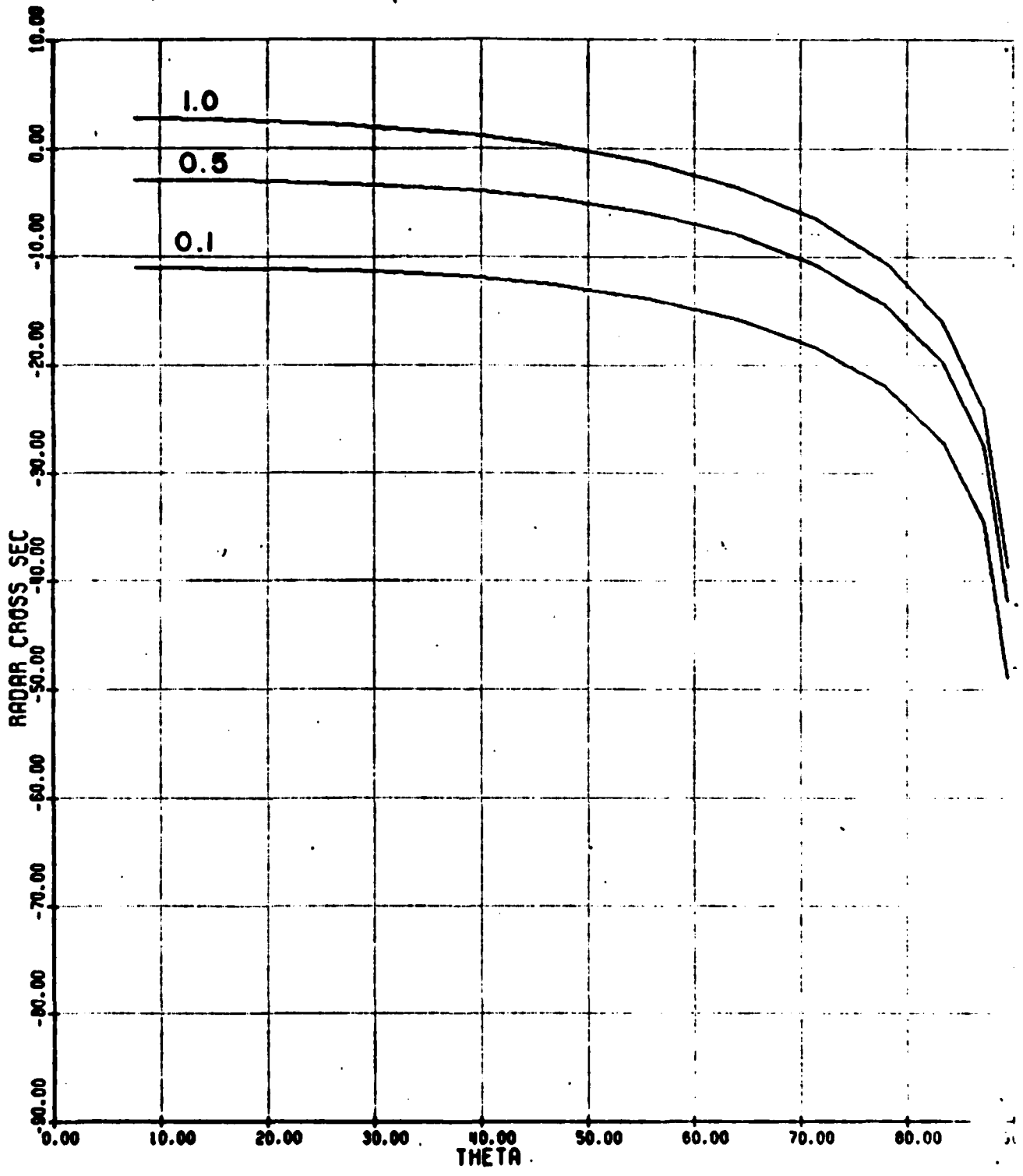

Fig. 15. Radar cross section with VV polarization versus incident angle with single scattering albedoes of .1, .5, and 1.0 for an optical depth of 5.0

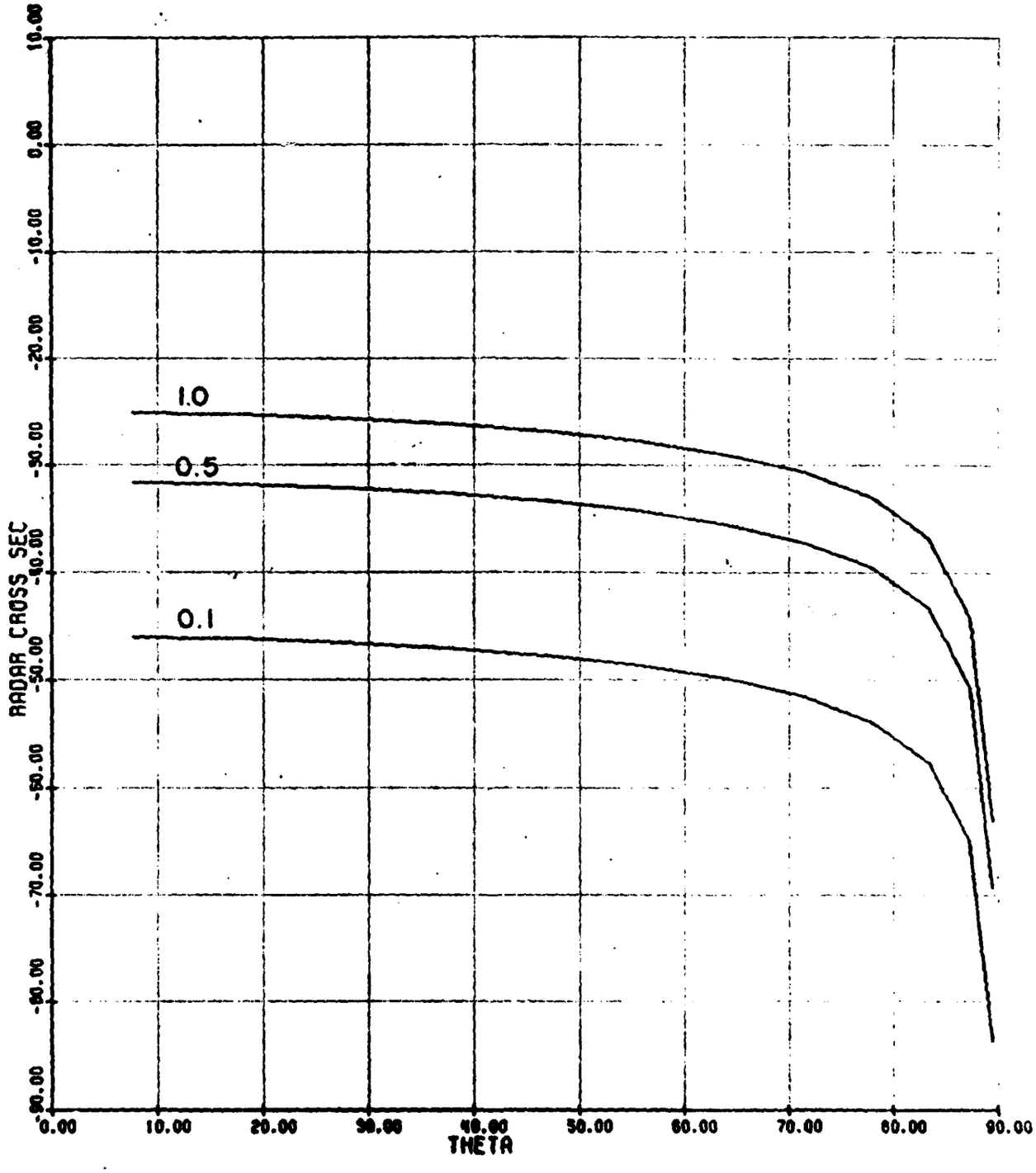

Fig. 16. Radar cross section with HV or VH polarization versus incident angle with single scattering albedoes of .1, .5, and 1.0 for an optical depth of .1.

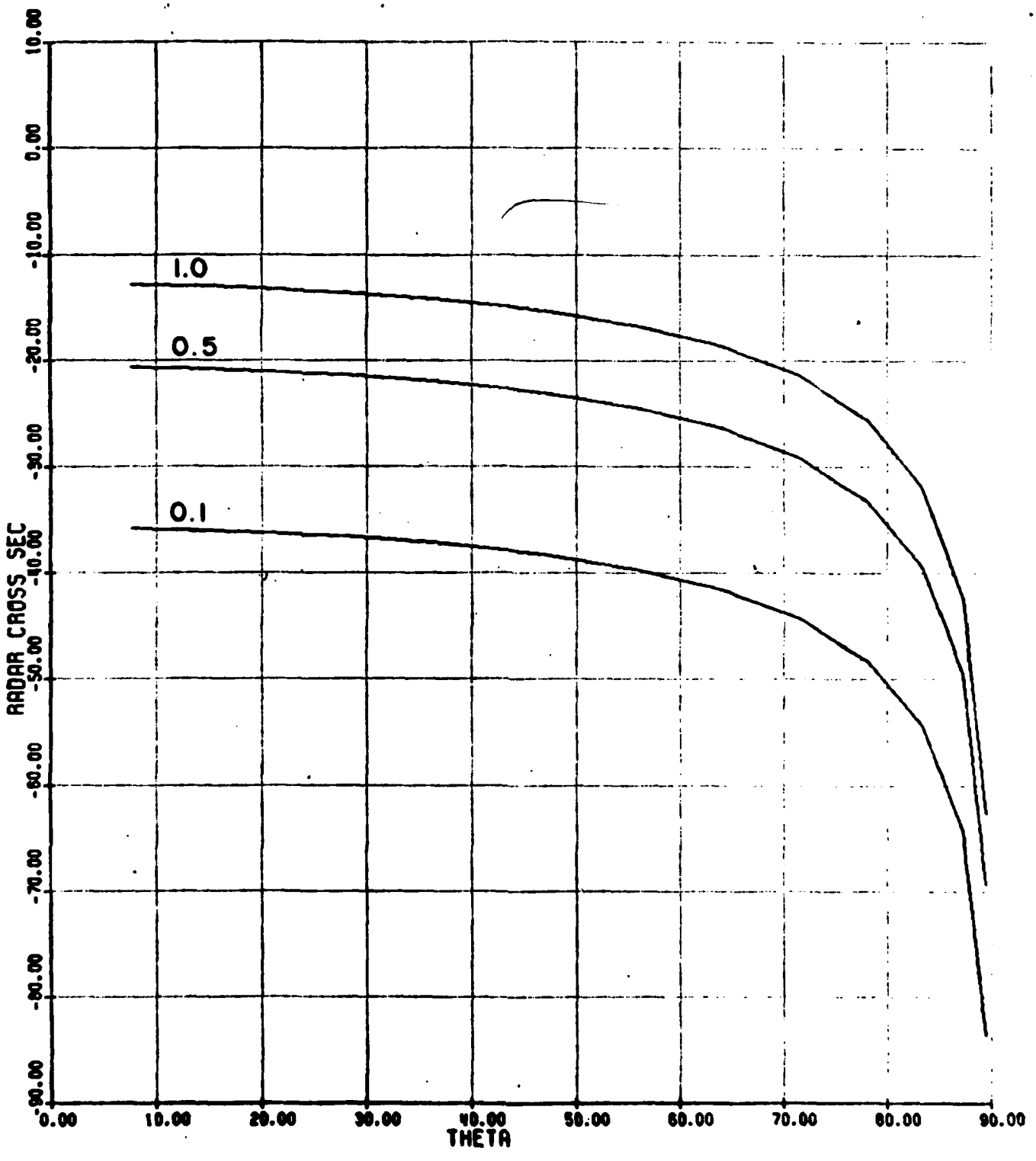

Fig. 17. Radar cross section with HV or VH polarization versus incident angle with single scattering albedoes of 1., .5, and 1.0 for an optical depth of .5.

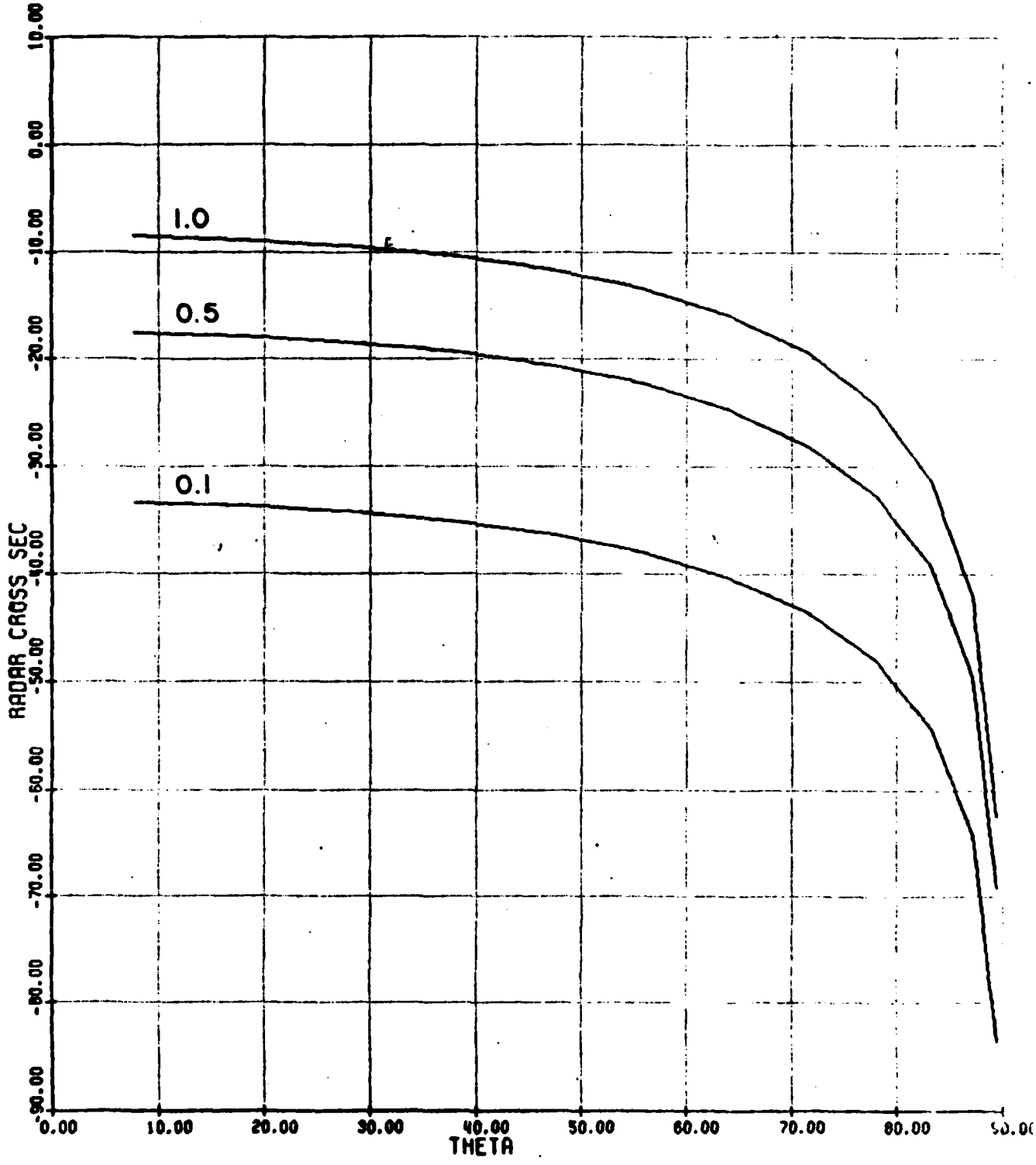

Fig. 18. Radar cross section with HV or VH polarization versus incident angle with single scattering albedoes of .1, .5, and 1.0 for an optical depth of 1.0.

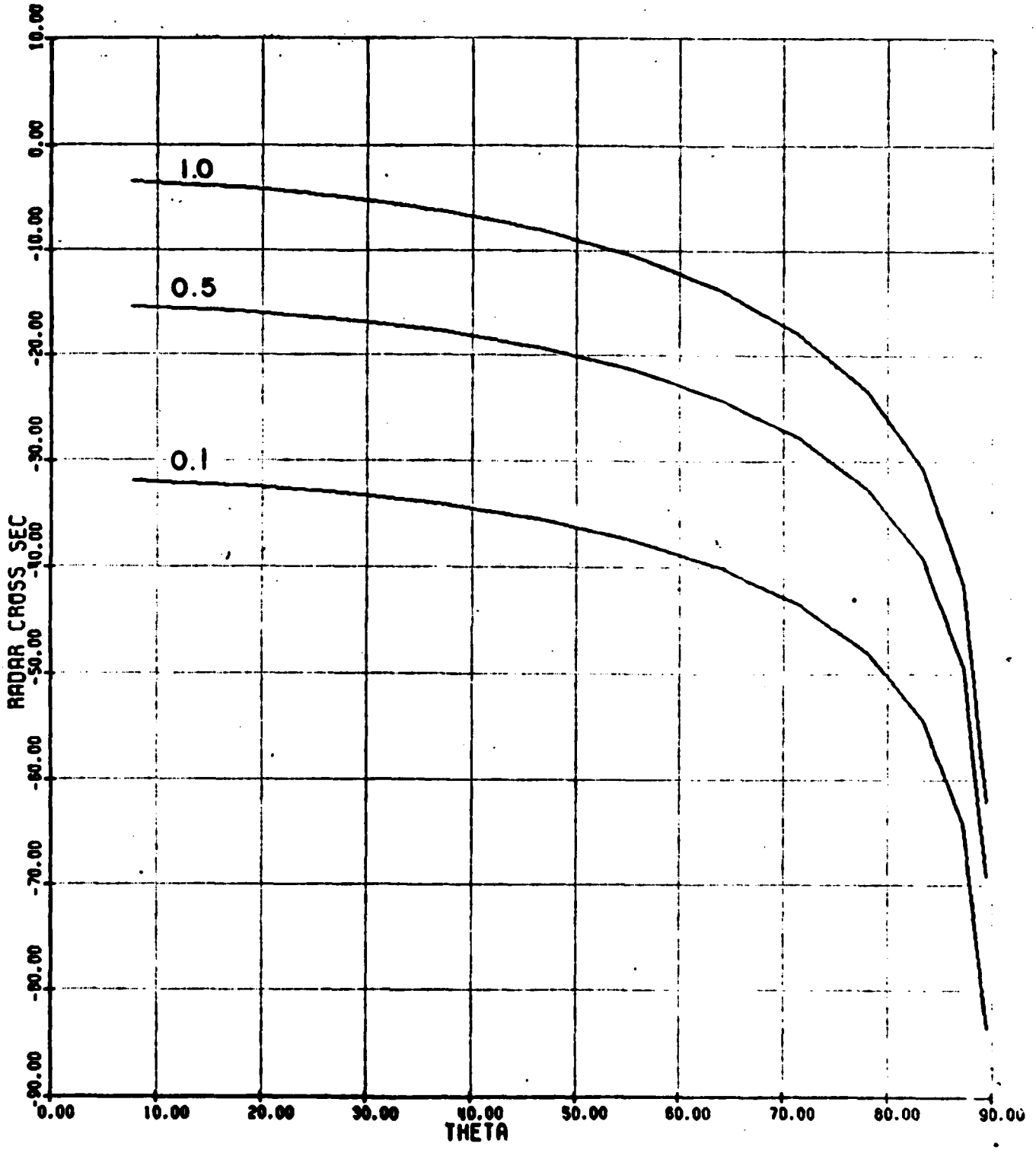

Fig. 19. Radar cross section with HV or VH polarization versus incident angle with single scattering albedoes of .1, .5, and 1.0 for an optical depth of 5.0.

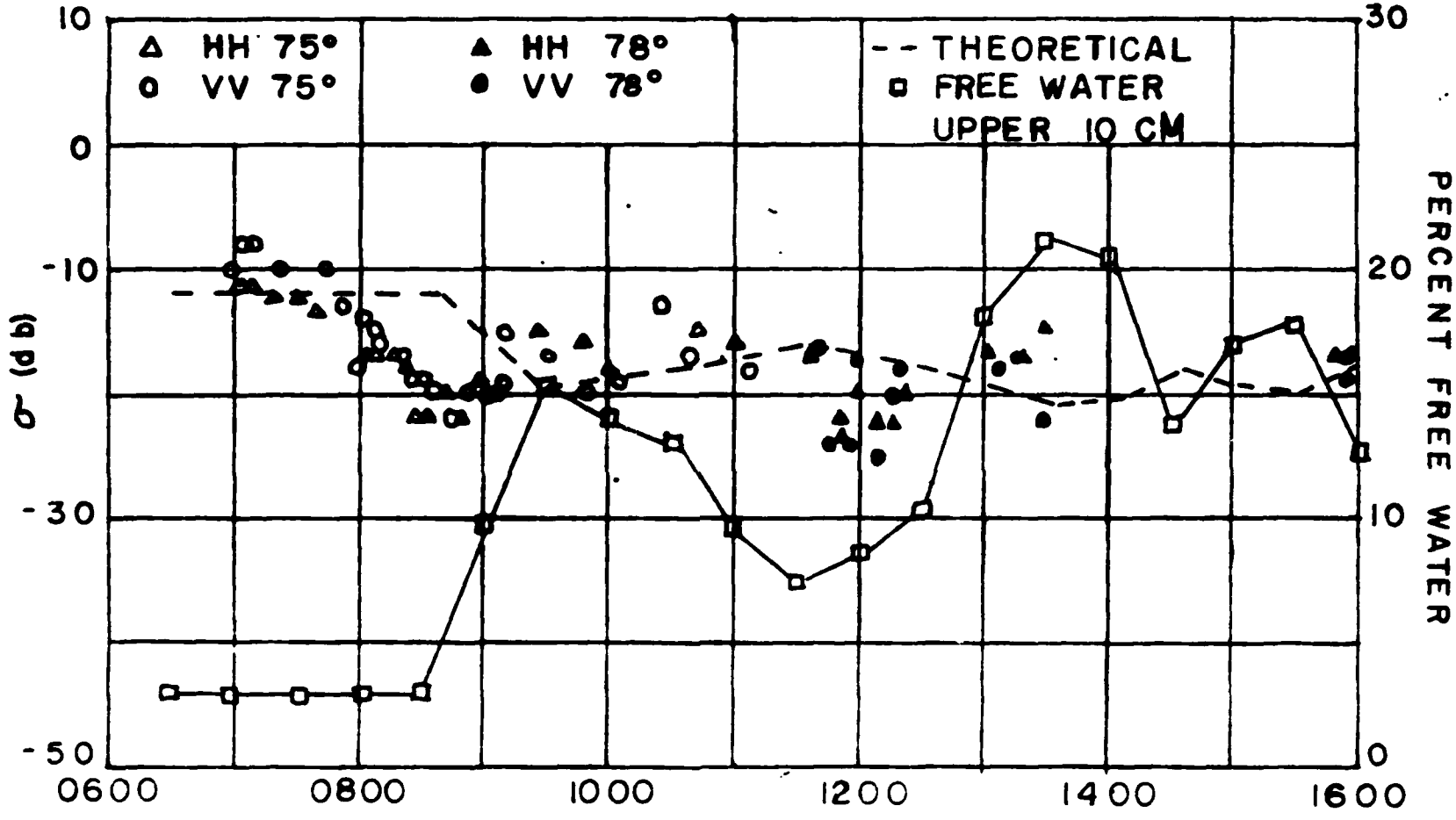

Fig. 20. Diurnal variation in the theoretical and experimental radar cross section at 35.0 GHz, and the diurnal variation in percent free water.

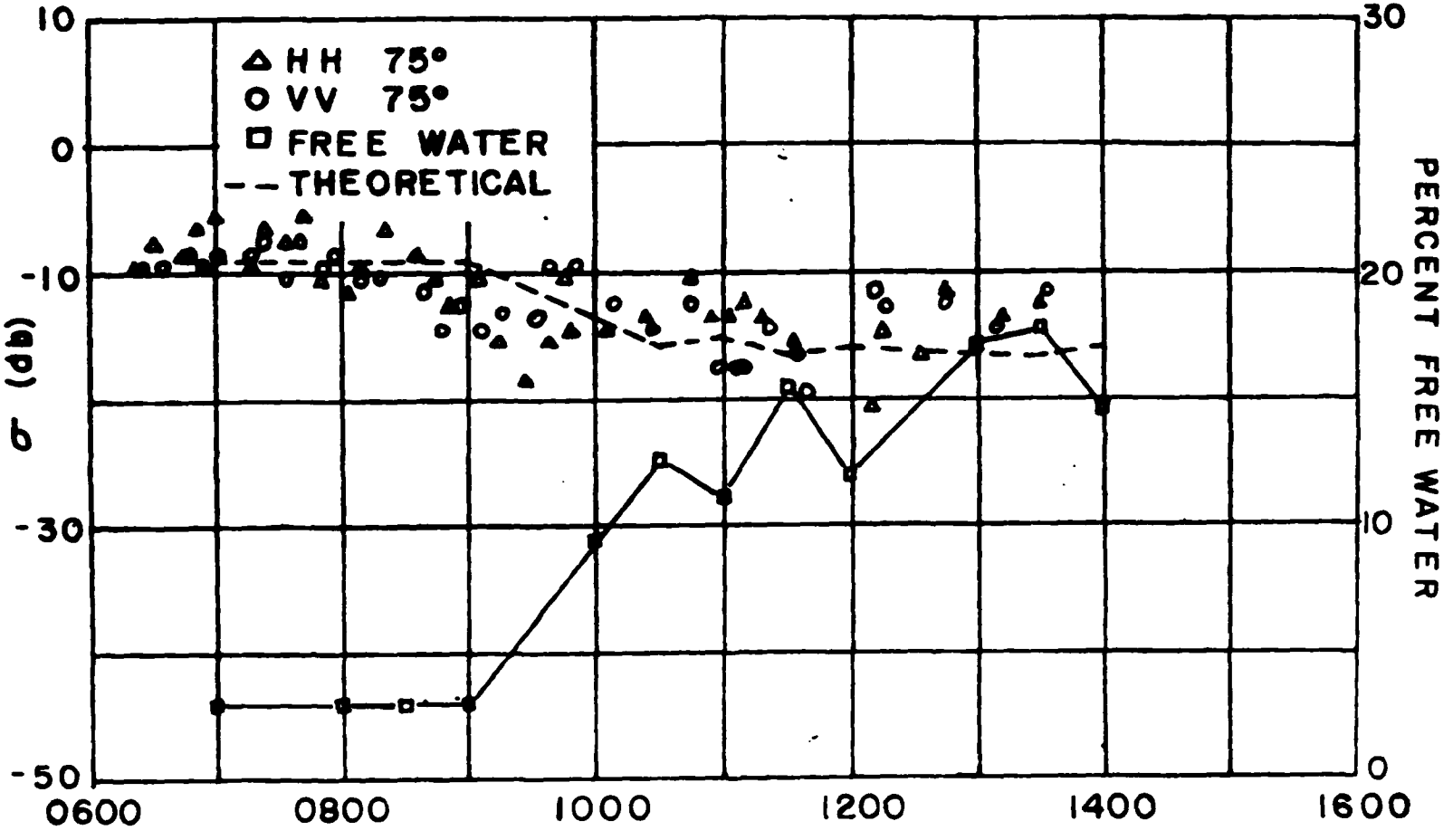

Fig. 21. Diurnal variation in the theoretical and experimental radar cross section at 35.0 GHz, and the diurnal variation in percent free water.

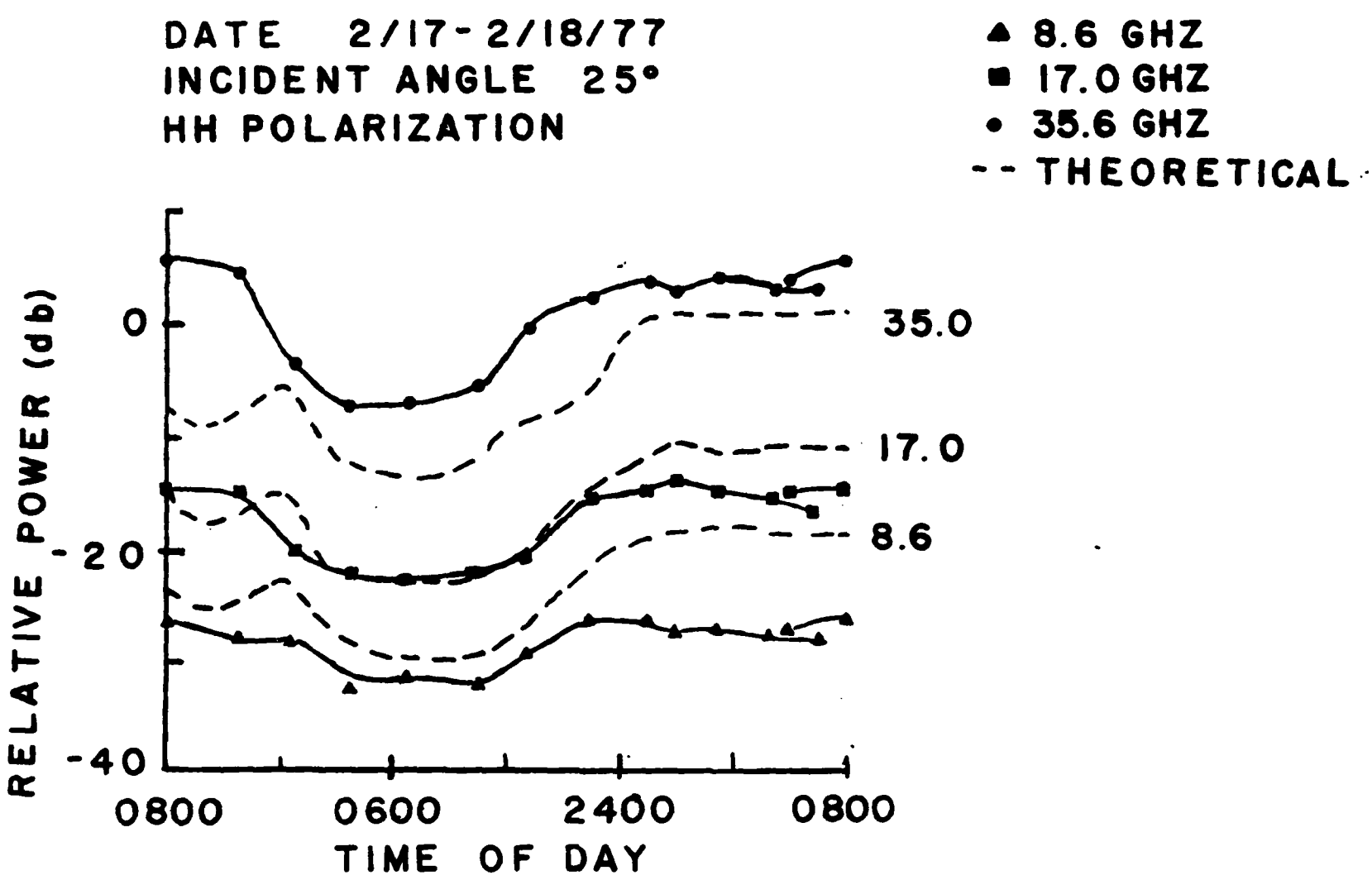

Fig. 22. Diurnal variation in experimental and theoretical power backscattered at frequencies of 8.6, 17.0, and 35.0 GHz on 2/27 - 2/18.

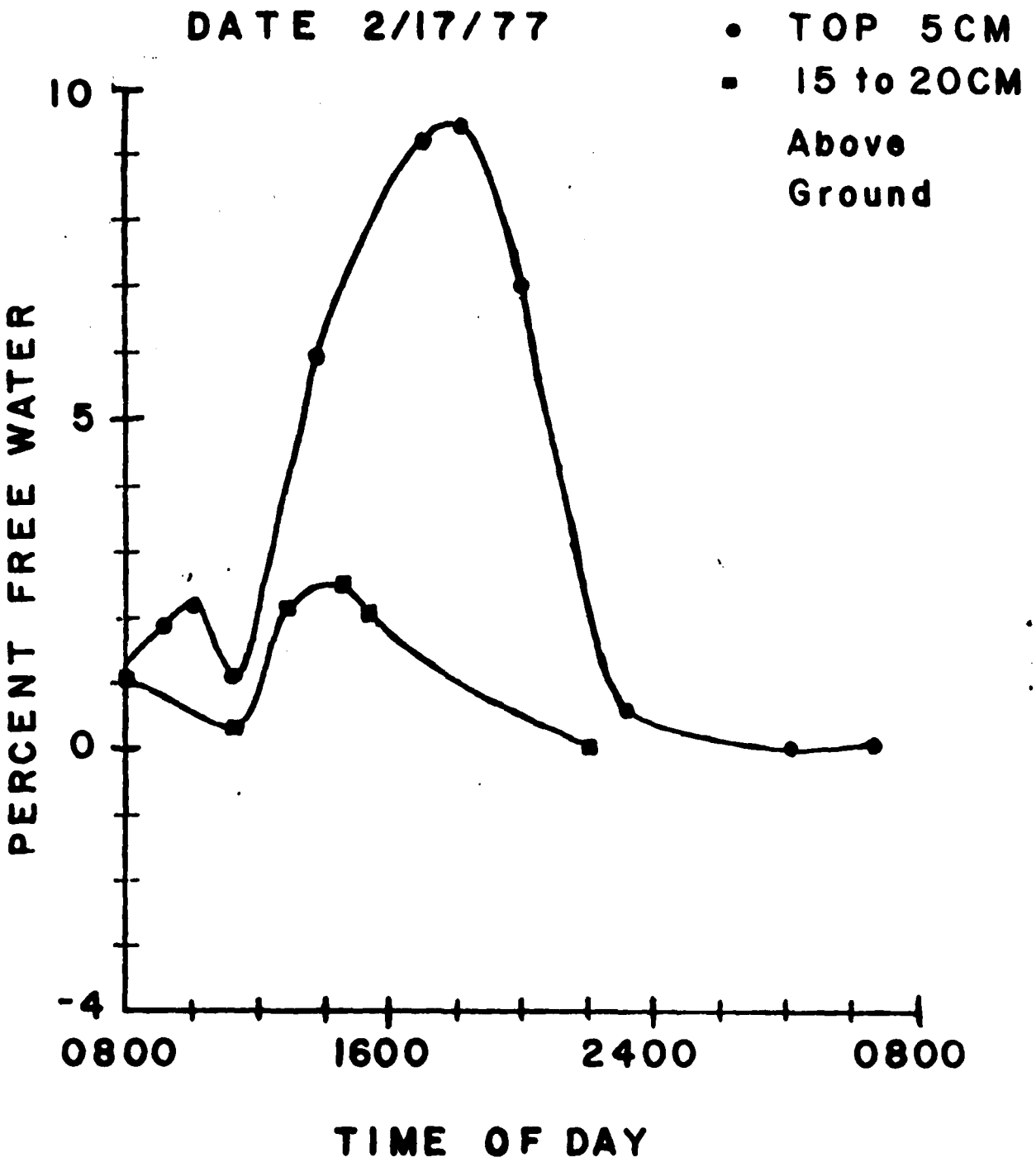

Fig. 23. Diurnal variation in percent free water on 2/17 - 2/18 for Fig. 22.